Title

Cytoplasmic TDP-43 De-mixing Independent of Stress Granules Drives Inhibition of Nuclear Import, Loss of Nuclear TDP-43, and Cell Death

Journal

Neuron, 102(2)

ISSN

0896-6273

Authors

Gasset-Rosa, Fatima
Lu, Shan
Yu, Haiyang
et al.

Publication Date

2019-04-01

DOI

10.1016/j.neuron.2019.02.038

Peer reviewed

HHS Public Access

Author manuscript

Neuron. Author manuscript; available in PMC 2020 April 17.

Published in final edited form as:

Neuron. 2019 April 17; 102(2): 339–357.e7. doi:10.1016/j.neuron.2019.02.038.

Cytoplasmic TDP-43 de-mixing independent of stress granules drives inhibition of nuclear import, loss of nuclear TDP-43, and cell death

Fatima Gasset-Rosa[1,*], **Shan Lu**[1,*], **Haiyang Yu**[1,*], **Cong Chen**[1,*], **Zevik Melamed**[1], **Lin Guo**[3], **James Shorter**[3], **Sandrine Da Cruz**[1,**], and **Don W. Cleveland**[1,2,**]

[1]Ludwig Institute for Cancer Research, University of California at San Diego, La Jolla, CA 92093

[2]Department of Cellular and Molecular Medicine, University of California at San Diego, La Jolla, CA 92093

[3]Department of Biochemistry & Biophysics, University of Pennsylvania, Philadelphia, PA 19104-6059

Abstract

While cytoplasmic aggregation of TDP-43 is a pathological hallmark of amyotrophic lateral sclerosis and frontotemporal dementia, how aggregates form and what drives its nuclear clearance have not been determined. Here we show that TDP-43 at its endogenous level undergoes liquid-liquid phase separation (LLPS) within nuclei in multiple cell types. Increased concentration of TDP-43 in the cytoplasm or transient exposure to sonicated amyloid-containing fibrils is shown to provoke long-lived liquid droplets of cytosolic TDP-43 whose assembly and maintenance are independent of conventional stress granules. Cytosolic liquid droplets of TDP-43 accumulate phosphorylated TDP-43 and rapidly convert into gels/solids in response to transient, arsenite-mediated stress. Cytoplasmic TDP-43 droplets slowly recruit importin-α and Nup62 and induce mislocalization of RanGap1, Ran, and Nup107, thereby provoking inhibition of nucleocytoplasmic transport, clearance of nuclear TDP-43, and cell death. These findings identify a neuronal cell death mechanism that can be initiated by transient-stress induced cytosolic de-mixing of TDP-43.

Graphical Abstract

**To whom correspondence should be addressed at sdacruz@ucsd.edu or dcleveland@ucsd.edu.

Author Contributions

F.G.-R., S.L., H.Y., C.C., S.D.C., and D.W.C. designed the research; F.G.-R., S.L., H.Y., C.C., S.D.C. and D.W.C. analyzed data; F.G.-R., S.L., H.Y., C.C. and Z.M. performed research; F.G.-R., S.L., H.Y., C.C., S.D.C. and D.W.C. wrote the text. L.G. and J.S. provided key reagents.

*These authors contributed equally

Declaration of interests

The authors declare no competing interests.

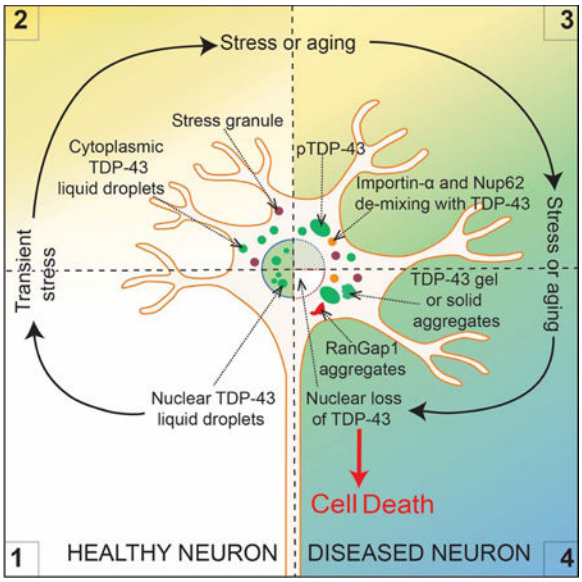

eTOC

TDP-43 aggregation is the major hallmark of multiple neurodegenerative diseases, including ALS and FTD. *Gasset-Rosa et al* demonstrate that transient stress induces long-lasting cytoplasmic TDP-43 de-mixing independent of stress granules, driving nuclear import defects, nuclear TDP-43 clearance, and cell death.

Keywords

TDP-43; RNA-binding proteins; low complexity domains; liquid-liquid phase separation; TDP-43 de-mixing; stress granules; iPSCs; motor neurons; neurodegeneration; ALS/FTD; nucleocytoplasmic transport

INTRODUCTION

Mislocalization, self-assembly, and aggregation of misfolded TAR DNA-binding protein 43 (TDP-43) in the cytoplasm of affected motor neurons is a common neuropathological hallmark of almost all cases of amyotrophic lateral sclerosis (ALS) (Neumann et al., 2006). Proteinaceous inclusions, containing misfolded aggregated proteins or fragments of them are also found in each of the major neurodegenerative disorders including Alzheimer's (AD), Parkinson's (PD), frontotemporal dementia (FTD), and Huntington's (HD) diseases (Chiti and Dobson, 2006). Many of the aggregated proteins contain intrinsically disordered protein domains that are enriched in, or composed of, only a few amino acids and are referred to as low complexity domains (LC). These domains display a sequence-intrinsic conformational heterogeneity (i.e., disorder) characteristic of intrinsically disordered proteins/regions (Boeynaems et al., 2018). LC domains are also present in yeast prion proteins, which have the ability to interconvert into amyloid-fibers (King et al., 2012). Prion-like LC domains are particularly abundant in RNA- and DNA-binding proteins, and their amino-acid composition has been conserved across evolution (King et al., 2012; Malinovska et al., 2013).

TDP-43 is a RNA-binding protein that localizes predominantly in the nucleus and is thought to shuttle between the cytoplasm and nucleus (Ayala et al., 2008). It forms abnormal cytoplasmic aggregates (Neumann et al., 2006) in neurons and glia in over 90% of ALS and 45% of FTD cases. These two progressive neurodegenerative diseases, which share genetic and pathological features (Ling et al., 2013), are without effective treatments to slow fatal disease progression (Taylor et al., 2016). Discovery of missense mutations in TDP-43 in patients with ALS or FTD (Rutherford et al., 2008; Sreedharan et al., 2008) demonstrated a direct link between genetic variants and TDP-43 pathology. Many mechanisms have been proposed to explain the abnormal cytosolic accumulation of TDP-43, and the progressive spreading of TDP-43 pathology.

TDP-43 contains a prion-like, LC domain that is glycine-, glutamine- and asparagine-rich, and is predominantly an intrinsically disordered region (IDR) (Conicella et al., 2016), which renders TDP-43 intrinsically aggregation prone (Johnson et al., 2009). Disordered domains of RNA-binding proteins can drive dynamic self-assembly into intracellular membrane-less organelles, including P granules (paranuclear granules in germline cells of *C. elegans*), nucleoli, and stress granules, each of which has been reported to fuse, minimize surface tension, and dynamically exchange components with the solution, all properties indicative of liquid-like behaviour (Brangwynne et al., 2009; Mitrea and Kriwacki, 2016). Correspondingly, phase separation might be the operational principle governing the formation of membrane-less organelles. A key unresolved issue is whether (and if so how) assembly into membrane-less organelles regulates/affects biological function(s) of their constituent proteins. Beyond that, phase-separated droplets have increasingly been implicated as crucibles for nucleation of pathologic protein aggregation since protein concentration is expected to be sharply increased within the droplets (Li et al., 2013; Ramaswami et al., 2013).

Prion-like LC domain-containing heterogeneous nuclear ribonucleoproteins (hnRNPs), such as FUS, hnRNPA1, TIA1 (other proteins whose mutation is causative of ALS/FTD) exhibit liquid-liquid phase separation (LLPS) as purified proteins *in vitro* (Burke et al., 2015; Mackenzie et al., 2017; Mateju et al., 2017; Molliex et al., 2015; Patel et al., 2015). TDP-43 has been reported to display aspects (round shaped morphology or fusion events) of liquid phase separation *in vitro* (Conicella et al., 2016; Ryan et al., 2018; Wang et al., 2018). Prolonged LLPS of purified FUS or repeated cycles of temperature-dependent de-mixing of mutant hnRNPA1 can induce conversion to a solid phase (Molliex et al., 2015; Patel et al., 2015), while expression of FUS variants with decreased ability to bind RNA can form solid-like aggregates in a cancer cell line (Maharana et al., 2018). The relevance of this altered phase behaviour is not established in disease, however, as in every reported instance the presence of other proteins or post-translationally modified variants inhibits liquid phase separation *in vitro* (Guo et al., 2018; Hofweber et al., 2018; Qamar et al., 2018; Yoshizawa et al., 2018). Only a handful of observations confirm LLPS properties of these RNPs in living cells, and in most examples de-mixing requires extreme conditions, including transient overexpression or degradation of total cellular RNA, or both (Gopal et al., 2017; Maharana et al., 2018; Wang et al., 2018).

No effort has succeeded in identifying whether TDP-43 undergoes liquid-liquid de-mixing in the cytoplasm - where pathological aggregates accumulate - and, if so, whether such de-mixing can trigger nuclear loss of TDP-43, conversion of TDP-43 to an aggregated state, or both. Here we identify intranuclear LLPS of native TDP-43 in multiple mammalian cells in cultured mouse cortical neurons and human iPSC-derived motor neurons. Arsenite-mediated stress is shown to induce TDP-43 de-mixing into cytoplasmic liquid droplets that are independent of stress granule components or formation and which rapidly convert to gels/solids that recruit phosphorylated TDP-43. Transient stress from exposure to fragmented amyloid-like fibrils induces endogenous TDP-43 de-mixing into cytosolic droplets which 1) form and persist for up to one month, 2) are independent of conventional stress granules, 3) accumulate phosphorylated TDP-43, 4) compromise nucleo-cytoplasmic transport, 4) slowly deplete nuclear TDP-43, and 5) ultimately elicit cell death.

RESULTS

Nuclear TDP-43 de-mixes under physiological conditions

While use of immunofluorescence has established that TDP-43 is primarily intranuclear, high resolution inspection (using N- or C-terminal antibodies) of endogenous TDP-43 revealed that it is not distributed diffusely in nucleoplasm, but rather forms rounded particles in both mouse and human cells, including cortical neurons from wild-type mouse brain, primary cultured mouse hippocampal neurons, human SH-SY5Y neuronal-like cells, U2OS, a human non-neuronal cell line, and motor neurons induced from human pluripotent stem cells (iPSCs) (Fig. 1A). An apparently de-mixed distribution was confirmed by imaging directly fluorescently tagged TDP-43 expressed at levels equal to or below the normal endogenous level (Fig. S1). Accumulation of 1) an amino-terminally EYFP-tagged TDP-43 (^{EYFP}TDP-43) to about one third the level of endogenous TDP-43 (Fig. S1A,B) or 2) a carboxy-terminally mRuby2-tagged TDP-43 (TDP-43^{mRuby2}) replacing endogenous TDP-43 (Fig. S1C) yielded between 5 and 50 rounded, droplet-like particles of 0.2–1 μm diameter in each nucleus (Fig. 1B). Similar rounded particles were found (Fig. 1B) in SH-SY5Y cells that had been genome edited at both TDP-43 alleles to encode fluorescently tagged TDP-43 (TDP-43^{sEGFP}), a variant which confers the essential functions of TDP-43 (Fig. S1D,E).

Live cell imaging was used to determine that these intranuclear TDP-43 particles have liquid-like properties. Fusion events could be observed frequently (see for example the fusion of two ^{EYFP}TDP-43 droplets labelled with green or red arrowheads in Fig. 1C,D) observed within a 10 second period of monitoring in neuron-like SH-SY5Y cells. Fluorescence recovery after photobleaching of whole ^{EYFP}TDP-43-containing droplets in SH-SY5Y revealed rapid recovery (to ~70% of original intensity) in <10 seconds (Fig. 1E,F), indicating fast molecular exchange of TDP-43 molecules between droplets and nucleoplasm. Internal molecular dynamics were five times faster, with fluorescence intensity re-equilibrated within 2 seconds following half-droplet bleaching (Fig. 1G). Fusion events were also documented for TDP-43^{mRuby2}- and TDP43^{EGFP}-containing droplets in U2OS or SH-SY5Y cells (Fig. 1H and S1F, respectively). Fission events were also observed (Fig. 1H, right panel), albeit at much lower frequency. As expected for LLPS, after photo-bleaching half of a nucleus, fluorescent intensity of TDP-43 recovered in the bleached half within 140

seconds, with a corresponding decrease in intensity in the unbleached half (Fig. 1I,J). Thus, TDP-43 phase separates in normal physiological conditions into intranuclear liquid droplets in which TDP-43 molecules dynamically move into and out of the droplets.

Concentration-dependent TDP-43 de-mixing in the cytoplasm

To mimic the increased accumulation of cytoplasmic TDP-43 during aging expected from the known age-dependent loss of nuclear pore components (D'Angelo et al., 2009), fluorescently-tagged TDP-43 with a disrupted NLS (TDP-43$^{\Delta NLS\text{-}Clover}$) was expressed using a doxycycline-inducible system in human U2OS cells that also stably express TDP-43^{mRuby2} (Fig. 2A) at endogenous TDP-43 level (Fig. S1C). Induction of TDP-43$^{\Delta NLS\text{-}Clover}$ produced a range of accumulation of cytoplasmic TDP-43 in individual cells, with Clover (and mRuby2) fluorescence providing a direct readout of TDP-43 level (Fig. 2B,C). Increased accumulation of cytoplasmic TDP-43 was sufficient to induce its de-mixing into 1–3 μm spherical, cytoplasmic particles (Fig. 2B) that 1) over time recruited the initially nuclear TDP-43^{mRuby2} (Fig. 2B) and 2) underwent fusions and fissions (Fig. 2D). TDP-43 cytoplasmic droplets remained liquid over extended periods, with rapid and efficient (70%) recovery (within 2 or 4 minutes, respectively) after complete or partial photobleaching (Fig. 2E,F). Thus, an increased level of cytoplasmic TDP-43 is sufficient to induce its de-mixing in the cytoplasm.

TDP-43 cytoplasmic de-mixing into liquid droplets

To determine if nuclear TDP-43 could redistribute to the cytoplasm and de-mix, we genetically-edited both TDP-43 alleles in SH-SY5Y cells to express physiological levels of wild-type TDP-43 fused to a green fluorescent protein (TDP-43^{EGFP}) (Fig. S1D,E). Non-dividing neuronal-like (SH-SY5Y) cells were then transiently exposed to fragmented amyloid-like containing fibrils. mCherry tagged recombinant TDP-43 (or FUS) was purified (Fig. S2A) and incubated for 24 hours at 20°C. Both self-assembled into fibrils whose appearance (Fig. 2H, S2B) was highly similar to amyloid-like fibrils (Rambaran and Serpell, 2008). After sonication, the fragmented fibrils (~20 nm in size) were added to the culture media of SH-SY5Y cells expressing TDP-43^{EGFP} from both endogenous TDP-43 alleles (Fig. 2G,H, S2B). As expected, without fibril addition TDP-43^{EGFP} remained nuclear without cytoplasmic liquid-like structures in non-cycling cells arrested in the G1 cell cycle phase (Fig. S2C).

After transient addition of TDP-43 sonicated fibrils (Fig. 2G,H), time-lapse imaging (both confocal and deconvolution) was used to 1) determine that fibril fragments were internalized within 12 hours, 2) follow the fate of the fibrils, and 3) determine localization of TDP-43^{EGFP} expressed at endogenous levels. At early times, fragmented TDP-43 fibrils accumulated in the cytoplasm but did not yield detectable TDP-43^{EGFP} recruitment (Fig. 2I). However, within 10 days, TDP-43^{EGFP} mislocalized to round, apparently de-mixed cytoplasmic droplets (Fig. S2D) and by 1 month most remaining cells accumulated TDP-43^{EGFP} cytoplasmic particles accompanied by depletion of nuclear TDP-43 (Fig. 2I). Cytoplasmic TDP-43 particles were confirmed by immunostaining with TDP-43 antibody (Fig. S2E). A parallel experiment with addition of FUS^{mCherry} particles (Fig. S2B) yielded

almost identical redistribution and apparent de-mixing of TDP-43^{EYFP} expressed at endogenous levels (Fig. 2J).

Recovery dynamics after photobleaching were used to determine that one month after their induction TDP-43 cytoplasmic particles represented LLPS, with rapid exchange with soluble TDP-43 in the cytoplasm driving fluorescence recovery within 25 seconds of full or focal photobleaching of single particles (Fig. 2K,L). Moreover, these old cytoplasmic droplets containing TDP-43 underwent frequent fusion (two examples are shown in Fig. 2M) and rarer fission events (Fig. S2F), indicative of LLPS. Younger droplets (accumulated 10 days after fibril exposure) displayed ~2.5 fold faster recovery.

Cytoplasmic TDP-43 liquid de-mixing independent of stress granules

To determine if endogenous untagged, wild type TDP-43 can be induced to de-mix in the cytoplasm, we exposed non-dividing neuronal-like SH-SY5Y cells to fragmented TDP-43 or FUS particles (Fig. 3A-D). Within 24 hours, a proportion of initially nuclear TDP-43 (Fig. 3E) accumulated in spherical, cytoplasmic particles many of which (see white arrows, top row, Fig. 3E) had undetectable levels of the fragmented TDP-43 or FUS fibrils, respectively. Indeed, no fibril fragments of TDP-43 or FUS could be detected within 4 days after their removal from the media, although in the majority (60%) of cells a proportion of endogenous TDP-43 remained in a series of round (~1 μm diameter) cytoplasmic particles (Fig. 3E,F). This apparent de-mixing of TDP-43 was still present a month after fibril exposure, more than 3 weeks after fibrils could no longer be detected (Fig. 3E), with the number of apparent droplets increasing 3 fold in a time-dependent manner (Fig. 3F). In all cases and time points, TDP-43 remained nuclear and without cytoplasmic particles in untreated cells (Fig. 3B) or cells treated with sonicated fragments of fibrils assembled from superoxide dismutase (SOD1) (Fig. S3B,C).

The cytoplasmic, de-mixed TDP-43 droplets induced by transient exposure to TDP-43 or FUS particles were very different from conventional stress granules, which assemble in response to heat or oxidative stresses and have been proposed to be the crucibles for pathological inclusion formation (Li et al., 2013). With very rare exceptions, no classical stress granule marker (TIA1, G3BP1, or UBAP2L) could be detected in fibril-induced TDP-43-containing droplets (Fig. 3G). Further, when stress granules were induced by exposure of the cells to sodium arsenite (Fig. S3D), little, if any, endogenously expressed TDP-43 was recruited to the resultant stress granules containing TIA1 or G3BP1 (Fig. 3H). Similarly, no stress granule component (e.g., TIA1 – Fig. S3E,F) could be detected in de-mixed, fluorescently tagged TDP-43 (TDP-43^{EGFP}) produced from the endogenous TDP-43 alleles, even after cell exposure to arsenite (Fig. S3F). Moreover, by one month, there was obvious nuclear clearing of TDP-43 in a proportion (~5%) of cells with fibril-induced cytoplasmic TDP-43 particles (Fig. 3I), indicating that an external amyloid-like particle induced re-localization of wild type endogenous TDP-43 to spherical, cytoplasmic particles can drive loss of nuclear TDP-43 function.

We next followed the kinetics of TDP-43 de-mixing in response to a high (250 μM) dose of sodium arsenite. Conventional stress granules marked by UBAP2L (Fig. 4A,B) or G3BP1 (Fig. 4A,D) formed within 20 minutes and recruited a proportion of an initially diffusely

localized cytoplasmic TDP-43$^{\Delta NLS\text{-}Clover}$ (Fig. 4B). By 40 minutes, most cells accumulated stress granules into which a small proportion of TDP-43 was recruited (Fig. 4B,C). However, by 50 minutes new rounded, cytoplasmic assemblies of TDP-43$^{\Delta NLS\text{-}Clover}$ began forming which did not contain UBAP2L (see arrowheads, Fig. 4B). By 90 minutes, most cytoplasmic TDP-43 (including the proportion initially recruited to stress granules) had redistributed into the new cytoplasmic droplets (Fig. 4B) in ~90% of the cells (Fig. 4C), despite continued presence of arsenite and UBAP2L- or G3BP1-containing stress granules (Fig. 4B,D). These findings are consistent with observations that the recruitment of a small proportion of full length TDP-43 to stress granules and that this can be enhanced by poly(ADP-ribose) binding to the TDP-43 nuclear-localization sequence (McGurk et al., 2018). Untagged cytoplasmic TDP-43$^{\Delta NLS}$ showed the same apparent arsenite-induced de-mixing behaviour without recruitment of stress granule components (Fig. S4A,B). Furthermore, application of cycloheximide before arsenite treatment abolished stress granule formation (as expected) but had no effect on the timing or extent of TDP-43 assembly into rounded cytoplasmic droplets (Fig. 4E). Addition of arsenite to a level too low to induce stress granules still provoked droplets of TDP-43$^{\Delta NLS\text{-}Clover}$ (Fig. 4F), consistent with extended low dose arsenite treatment producing cytoplasmic TDP-43-containing particles that are independent of stress granules and their components (McGurk et al., 2018).

Photobleaching was used to test molecular exchange within the TDP-43 spherical particles that do or do not contain stress granule markers and which formed in the cytoplasm in response to arsenite stress (Fig. 4G,H). Like UBAP2L itself, about half the TDP-43 initially recruited into rounded, UBAP2L-positive stress granules recovered rapidly after photobleaching (Fig. 4G,H), with kinetics similar to the previously reported dynamics of components of conventional stress granules (Molliex et al., 2015). Consistent with droplets formed by LLPS, similarly rapid recovery after photobleaching was seen for about half the TDP-43 recruited into the rounded TDP-43 assemblies that formed 50 minutes after exposure to arsenite and which did not contain stress granule components (Fig. 4I,J).

Arsenite-induced gelling of de-mixed cytoplasmic TDP-43 droplets

While arsenite-induced stress granules (marked by UBAP2L) maintained liquid properties (Fig. 5A,B) throughout prolonged arsenite exposure, the initially liquid-like cytoplasmic TDP-43$^{\Delta NLS\text{-}Clover}$ droplets that formed without stress granule components (Fig. 4I,J) converted within an additional 30 min of arsenite exposure into gels/solids, with almost no intraparticle molecular exchange following partial or complete photobleaching (Fig. 5A-D). The particles did not contain detectable mRNA (Fig. S5C), EDC4-containing P body components (Fig. S5D), or p62 (Fig. S5E), but did acquire TDP-43 phosphorylated at serines 409 and 410 (Fig. S5B), as is found in human ALS/FTD pathology. Consistently, the proportion of insoluble TDP-43 increased with time of exposure to arsenite (Fig. S5A). Once converted, the particles remained gel/solid-like even after removal of arsenite (Fig. 5E,F), and recruited p62 with time (Fig. S5F).

TDP-43^{EGFP} droplets induced by transient exposure to sonicated fibrils of TDP-43 or FUS remained liquid for at least three weeks after initial droplet formation (Fig. 2K-M) without acquisition of amyloid oligomers detectable with the widely used A11 antibody (Fig. S5G,

left panel) that recognizes a peptide backbone epitope common to amyloid oligomers (Kayed et al., 2007) and also recognizes cytoplasmic TDP-43-containing “myogranules” in regenerating muscle cells (Vogler et al., 2018). However, within 30 minutes of exposure to sodium arsenite, the TDP-43^{EGFP} droplets quickly converted into a gelled state (Fig. 5G,H) remaining rounded, but with almost no intra-particle molecular exchange following photobleaching of a portion of a particle and almost no recruitment of new molecules from the cytoplasm after full particle photobleaching (Fig. 5H). Furthermore, eighty percent of cytoplasmic gel/solid-like TDP-43 particles acquired some amyloid-like character measured with the A11 antibody which recognizes a pre-amyloid oligomeric conformation (Fig. S5G, **right-lower panel**). In contrast, while almost all of the cytoplasmic TDP-43 de-mixed particles that persisted over one month without exposure to arsenite did not acquire detectable amyloid-oligomers (Fig. S5G, **right-upper panel**). Hence, arsenite mediates a structural conversion within TDP-43 droplets from weak self-interactions to gels/solids containing beta-sheet structure, whose incorporation is likely to slow dynamics of exchange with soluble TDP-43 and facilitate TDP-43 aggregation.

TDP-43 de-mixing in iPSC-derived motor neurons independent of stress granules

We next tested whether an increased level of cytoplasmic TDP-43 was sufficient to drive its de-mixing within human motor neurons (Fig. 6A). Forced expression of cytoplasmic TDP-43 in iPSC-derived motor neurons produced rounded cytoplasmic structures in the absence (Fig. 6B) or presence of a low dose of sodium arsenite (Fig. 6C), in both cases without stress granule assembly or recruitment of stress granule proteins (e.g., G3BP1 – Fig. 6B,C). In the absence of arsenite, the rounded TDP-43 particles were liquid-like (as indicated by fast fluorescence recovery after photobleaching - Fig. 6D,E). Low dose arsenite addition rapidly converted the TDP-43-containing droplets into gel/solid-like particles that did not recover after photobleaching (Fig. 6F,G). Thus, elevation of cytoplasmic TDP-43 level in human motor neurons is sufficient to drive cytoplasmic LLPS of TDP-43 independently of the principal components of stress granules or stress granule assembly.

Cytoplasmic de-mixing progressively depletes nuclear TDP-43 and induces cell death

We next evaluated the kinetics and longevity of cytoplasmic TDP-43 LLPS induced in the cytoplasm by transient exposure to sonicated amyloid-like fibrils and whether continued de-mixing affected cell viability. Fragmented fibrils were transiently added to the culture media of non-cycling, neuronal SH-SY5Y cells genome edited to express TDP-43^{EGFP} from both endogenous TDP-43 alleles (Fig. 7A). Within 4 days, TDP-43^{EGFP} partially re-localized into rounded cytoplasmic particles, many of which had undetectable fibrils (e.g., see white arrow, column 2, Fig. 7B). The number and size of the cytoplasmic TDP-43-containing particles increased with time (Fig. 3F, 7B). Seven days after transient fibril exposure, 50% of the cells had rounded cytoplasmic TDP-43 droplets, but no remaining fibrils could be detected in any cell (Fig. 7B). Beginning ~10 days after fibril exposure, cytoplasmic LLPS of TDP-43 was accompanied by nuclear clearing of TDP-43 in some cells. By 1 month, most remaining cells accumulated TDP-43^{EGFP} cytoplasmic particles with nuclear TDP-43 depletion (Fig. 7B). The TDP-43 droplets did not contain detectable RNA (Fig. S6A,B,D) and were independent of arsenite-induced poly-A RNA-containing stress granules (Fig. S6C). The one month old cytoplasmic TDP-43 LLPS droplets induced by amyloid-like particles recruited

phospho-TDP-43 (Fig. 7E), but not ubiquitin or the autophagy adaptor protein p62 (Brady et al., 2011) (Fig. S6F). While no cell death was seen within the first week, within two weeks after fibril exposure 60% of cells had died, with most of the remaining cells displaying both cytoplasmic LLPS and nuclear clearance of TDP-43. By 6 weeks, there were almost no cell survivors (Fig. 7C,D).

Disrupted nucleocytoplasmic transport enhances nuclear depletion of TDP-43

Recognizing that defects in nuclear membrane structure and/or nucleocytoplasmic transport have been reported in the nervous systems of patients with ALS caused by hexanucleotide repeat expansion in *C9orf72* (Freibaum et al., 2015; Jovicic et al., 2015; Zhang et al., 2015) or mutation in SOD1 (Kinoshita et al., 2009) and in mouse models of TDP-43 or SOD1 mutant-mediated disease (Chou et al., 2018; Ditsworth et al., 2017; Zhang et al., 2006), we examined the integrity of the nuclear membrane and nuclear import in non-cycling SH-SY5Y neuronal cells with cytoplasmic LLPS of TDP-43. Transient exposure to amyloid-like particles provoked gradual retention in the cytoplasm of components critical for nucleocytoplasmic transport (Fig. 8A-D). Cytoplasmic mislocalization of RanGAP1, the Ran GTPase-activating protein 1 required for Ran-dependent nuclear import and export, was found in some cells within one week (Fig. 8B). RanGap1 mislocalization increased in a time-dependent manner, with 70% of cells accumulating RanGap1 in large, cytoplasmic inclusions within a month after fibril exposure (Fig. 8C), along with progressive accumulation of de-mixed TDP-43 in the cytoplasm.

Imported cargo is released after import into the nucleus when importin transporters interact with intranuclear Ran-GTP. Correspondingly, high levels of intranuclear Ran-GTP are essential for active transport through nuclear pore complexes (NPCs) and for defining nucleocytoplasmic transport directionality. Consistent with disruption in nuclear import, continuing LLPS of fragmented fibril-induced TDP-43 was accompanied by Ran accumulation into small cytoplasmic inclusions (Fig. 8D). Furthermore, after one month of TDP-43 LLPS, two components of nuclear pores (Nup107 and Nup62) were found accumulated in cytoplasmic particles, with one (Nup62) co-recruited into rounded TDP-43-containing droplets (see white arrows, Fig. 8D), indicative of phase separation of Nup62 together with TDP-43. Similarly, FUS and hnRNPA1 also redistributed to the cytoplasm (Fig. S7A-B), with hnRNPA1 also recruited into TDP-43 de-mixed particles (Fig. S7B, **lower panel**). The evidence that hnRNPA1 is co-recruited with TDP-43 LLPS is in accordance with a report that the LCD of TDP-43 phase separates with the LCD of hnRNPA2 *in vitro* (Ryan et al., 2018). Finally, the nuclear import transporter importin-α, which is not only responsible for recognizing the TDP-43 nuclear localization signal but has also been reported to function as a cytosolic protein chaperone (Jakel et al., 2002) that together with karyopherin-β1 can dissolve TDP-43 amyloid-like fibrils *in vitro* (Guo et al., 2018), was also phase separated into large the cytoplasmic TDP-43-containing droplets (see white arrows, Fig. 8D, **lower panels**). Overall, induction of cytoplasmic TDP-43 LLPS is sufficient over a timescale of weeks to drive a feed-forward mechanism compromising nucleo-cytoplasm transport and exacerbating loss of nuclear TDP-43 (Fig. 8E).

DISCUSSION

Here we demonstrate that LLPS reflects a normal TDP-43 behaviour *in vivo,* as we show that it is apparently de-mixed intranuclearly in cortical neurons in the mouse brain and multiple examples in cell culture. TDP-43 molecules exhibit fast (within seconds) dynamic exchange within the liquid droplets as well as between the droplets and an aqueous pool. Intranuclear TDP-43 thus recapitulates the characteristics of what has been defined as a liquid produced by LLPS (Boeynaems et al., 2018; Brangwynne et al., 2009). We also show that beyond intranuclear de-mixing, TDP-43 can be induced to de-mix in the cytoplasm 1) when cytoplasmic TDP-43 levels are elevated, 2) in response to transient exposure to amyloid-like fibrillar TDP-43 or FUS, or 3) following exposure to sodium arsenite. In all cases, TDP-43 de-mixes initially into liquid droplets (with rapid molecular exchange with soluble TDP-43 molecules), but converts to rounded gel/solid-like structures with arsenite exposure.

The interaction of TDP-43 (Afroz et al., 2017; Becker et al., 2017; Khalfallah et al., 2018; Li et al., 2013; Ramaswami et al., 2013) or FUS (Guo et al., 2018; Hofweber et al., 2018; Li et al., 2013; Marrone et al., 2018; Zhang et al., 2018) with stress granules has repeatedly been proposed to be a means to enhance their subsequent aggregation. In contrast, we have found that cytoplasmic LLPS of TDP-43 can be independent of components of stress granules and stress granule assembly, despite initial recruitment of a small proportion of TDP-43 into stress granules induced with a high dose of sodium arsenite. Perhaps most provocatively, simply increasing cytoplasmic TDP-43 (as would be driven by the known age-dependent reduction in nuclear import (D'Angelo et al., 2009; Mertens et al., 2015)) or transient exposure to fibrillar fragments of aggregated TDP-43 (or FUS) recruits TDP-43 into de-mixed cytoplasmic liquid droplets that are independent of stress granules and which slowly deplete nuclear TDP-43 and induce cell death over a six-week period. Added to the complexity of TDP-43 de-mixing, it is not established whether the cytoplasmic particles we identify here are similar to axonally transported TDP-43-containing droplets that form in cortical neurons following TDP-43 overexpression (Gopal et al., 2017). Identifying the constituents of each of these TDP-43-containing compartments is an unsolved question of high interest for elucidating possible functions carried out within such compartments.

A prominent hallmark of ALS and FTD is nuclear clearance and cytoplasmic TDP-43 aggregation in neurons and glia within the central nervous systems (Neumann et al., 2006). Here, we have established that increased TDP-43 concentration in the cytoplasm or application of either of two transient stresses can induce long-lasting LLPS of endogenous TDP-43. While much attention has focused on the relationship of stress granules with disease-related RNA binding protein aggregation (Becker et al., 2017; Jain et al., 2018; Mackenzie et al., 2017; Markmiller et al., 2018), our findings demonstrate that cytoplasmic de-mixing of TDP-43 can be independent of stress granule formation, with at most a small proportion of TDP-43 transiently recruited to stress granules. Recognizing that other RNA binding proteins have previously been reported to indirectly associate with TDP-43 through simultaneous binding to a common RNA (Coyne et al., 2015; Elden et al., 2010), it is plausible that transient association of a minority of TDP-43 molecules with stress granules is driven indirectly through TDP-43 binding to RNAs that are also bound to proteins directly

recruited to stress granules. In addition, TDP-43 can bind to poly(ADP-ribose) via its nuclear-localization sequence. Binding promotes TDP-43 recruitment to stress granules and delays the initial accumulation of disease-associated TDP-43 phosphorylation that accompanies sustained arsenite-mediated stress (McGurk et al., 2018). TDP-43 phase separation into droplets without conventional stress granule components is consistent with the near absence of evidence using immunohistochemistry and immunofluorescence of stress granule formation or co-localization of stress granule proteins with cytoplasmic TDP-43 aggregates in tissues from patients (Colombrita et al., 2009; Dormann et al., 2010; Liu-Yesucevitz et al., 2010; Mackenzie et al., 2017; McGurk et al., 2014; Neumann et al., 2007) or more recently from proteomic analysis of insoluble TDP-43 containing homogenates from ALS or FTD patients (Laferriere et al., 2019).

We have established that transient exposure to amyloid-like TDP-43 (or FUS) particles is sufficient to induce TDP-43 de-mixing into spherical liquid-liquid cytoplasmic droplets that ***1)*** can be stable for weeks and exhibit ***2)*** dynamic internal molecules, ***3)*** exchange with TDP-43 in the cytoplasm, ***4)*** fusion and fission events, and ***5)*** whose presence slowly depletes nuclear TDP-43 accompanied by reduced cell survival. [Nuclear TDP-43 depletion has also been reported when TDP-43 is co-recruited into polyglutamine repeat inclusions (Fuentealba et al., 2010).] Induced LLPS of TDP-43 is potentially mediated through modifications of it or its binding partners that affect the multivalent interactions that are generally thought to be the driving forces of protein phase separation (Dao et al., 2018; Li et al., 2012; Molliex et al., 2015). Evidence from multiple investigators has supported post-translational modifications and/or binding partners that can act to suppress or enhance de-mixing of FUS (Guo et al., 2018; Hofweber et al., 2018; Qamar et al., 2018; Yoshizawa et al., 2018). Here we show that a portion of TDP-43 within liquid cytoplasmic droplets is phosphorylated, suggesting that LLPS may represent the initial event which then matures to a gel-like solid state that ultimately nucleates TDP-43 aggregation.

A likely, disease-related stress is the reduction in nuclear import during normal aging (D'Angelo et al., 2009; Mertens et al., 2015; Scaffidi and Misteli, 2006), coupled with further import inhibition in different neurodegenerative diseases (Freibaum et al., 2015; Gasset-Rosa et al., 2017), including ALS (Boeynaems et al., 2016; Ditsworth et al., 2017; Freibaum et al., 2015; Jovicic et al., 2015; Zhang et al., 2018; Zhang et al., 2015). Here we demonstrate that major regulators of nucleocytoplasmic trafficking (RanGap1, Ran, Nup107 and Nup62) are abnormally localized as a consequence of induced cytoplasmic LLPS of TDP-43. While nuclear-import receptors including importin-α and karyopherin-β1 have been reported to prevent or reverse TDP-43 aggregation *in vitro* (Guo et al., 2018) (in addition to directly mediating nuclear import of TDP-43), we have found that induced LLPS of TDP-43 in the cytoplasm recruits importin-α, thereby producing an importin-α loss of function that will exacerbate nuclear import deficits. Co-recruitment of Nup62 and importin-α into TDP-43 droplets points to TDP-43 phase separation to be at least one driving force inducing inhibited nuclear import.

We note that reduced nuclear import will obligatorily disrupt the TDP-43 autoregulation pathway (Ayala et al., 2011; Polymenidou et al., 2011) which sets the level of new TDP-43 synthesis through the nuclear action of TDP-43 in the processing of its own pre-mRNA

(Polymenidou et al., 2011). Diminished nuclear TDP-43 function, coupled with increased cytoplasmic accumulation from inhibition of nuclear import, produces a feed-forward loop for driving increasing cytoplasmic TDP-43 accumulation, further exacerbating the disruption of its autoregulation pathway and producing even higher levels of cytoplasmic TDP-43. During aging, this would be expected to be sufficient to drive concentration-dependent cytoplasmic phase separation of TDP-43, which together with the loss of TDP-43 nuclear function ultimately drives cell death.

Lastly, our evidence has shown that beyond age-dependent loss of nuclear import, other stresses – including transient, extracellular contact with aggregated, amyloid-like fibrils of assembled TDP-43 or FUS – can trigger or contribute to de-mixing of TDP-43 in the cytoplasm. One of these stresses is likely to be a proteome imbalance generated by the altered protein abundances that arise from changes in the levels and/or splicing of >1500 mRNAs in the nervous system when TDP-43 is diminished (Polymenidou et al., 2011; Tollervey et al., 2011). Efforts to identify additional biological sources of such stress are now of high importance for establishing the cascade of events underlying age-dependent neurodegenerative diseases that have TDP-43 misaccumulation and aggregation as prominent features.

STAR Methods

TABLE OF RESOURCES (Attached)

CONTACT FOR REAGENT AND RESOURCE SHARING

Further information and requests for resources and reagents should be directed to and will be fulfilled by the Lead Contact, Don Cleveland: dcleveland@ucsd.edu

EXPERIMENTAL MODEL AND SUBJECT DETAILS

Mice—C57BL/6 mice were obtained from Charles River Laboratories (Cat# C57BL/6NCrl). Males were perfused in a 20% paraformaldehyde solution and tissues collected for imaging. Maintenance and experimental procedures were approved by the Institutional Animal Care and Use Committee of the University of California, San Diego.

Cells Lines

iPSC-derived motor neurons: Human iPSC cells, derived from peripheral blood mononuclear cells donated by a 58-year-old healthy Caucasian male, were generated by iXCells Biotechnologies and selected for normal karyotype with normal self-renewal and differentiation ability (Melamed et al., 2019). iPS cells were first differentiated into motor neuron precursors in 21 days and then further differentiated into motor neurons for another 7 days using a differentiation protocol patented by iXCells Biotechnologies (Provisional Application no. 14359–001-888) (Melamed et al., 2019). Then the cells were infected by lentivirus to express cytoplasmic TDP-43$^{\Delta NLS\text{-}GFP}$ under ubiquitin promoter as summarized in Figure 6.

Stable cell line construction: lentivirus infection and selection: HEK293T cells were used for packaging lentiviruses. Briefly, 0.5 ×10^6 per well of 293T cells were seeded in a 6-

well plate and cultured with DMEM medium (Thermo Fisher) supplemented with 10% FBS (Omega Scientific), 100 units/mL of penicillin, 100 μg/mL of streptomycin, and 250 ng/mL of Gibco Amphotericin B (Thermo Fisher). For lentiviral transfection, 1.5 μg of the lentiviral plasmid (constructs are labelled as lentivirus in Key Resources Table), 1 μg of pMD2.G and 0.5 μg of psPAX2 were inoculated to each well using Mirus transIT-X2 transfection reagent. Culture medium was changed to fresh medium at 4~24 hours post transfection. Two days after transfection, the culture medium was filtered through a 0.45 μm syringe filter to generate the viral soup. The viral soup containing 10~50 μg/mL protamine sulfate was added to U2OS or SH-SY5Y cells cultured in DMEM medium or in DMEM/F12 medium (Thermo Fisher) for infection. The viral soup was removed 24 hours after infection, and cells were passaged at least once before selection. Infected cells are selected based on the selection markers encoded by the lentivirus. For U2OS, the concentrations of the antibiotics used for selection were 200 μg/mL for neomycin (Thermo Fisher), 20 μg/mL for blasticidin (Thermo Fisher), 1 μg/mL for puromycin (Thermo Fisher). For SH-SY5Y cells, the concentrations were 400 μg/mL for neomycin, 10 μg/mL for blasticidin and 3 μg/mL for puromycin.

TDP-43 alleles were genetically modified in SH-SY5Y cells. A single guided RNA targeting TDP-43 was designed (Benchlin webtool) and cloned into pSpCas9 plasmid (px330-Addgene) (Cong et al., 2013) using the BbsWE restriction site. The sequence for guided RNA targeting TDP-43 is: GCTGGGGAATGTAGACAGTG. To promote homologous recombination, pSpCas9-gRNA plasmid was electroporated using Amaxa Nucleofactor (assay A-023) along with a template plasmid, containing two TDP-43 homology arms, each 800bp long, separated by AID-GFP segment that is adjacent upstream to the TDP-43 terminal codon. 48 hours following electroporation, cells were collected and dissociated using Accutase (Innovative Cell Technologies). GFP-positive cells were sorted and single-cell seeded into 96 wells plates using the SH800S Sony cell sorter. Individual clones were expanded and DNA was extracted for PCR amplification of TDP-43 genomic locus. Insertion of AID-GFP was finally confirmed by immunoblotting. The entire TDP-43 coding region was then sequenced to verify the absence of any additional DNA alteration.

METHOD DETAILS

Mice surgery and tissue preservation—Anesthetized animals (C57BL/6) were subjected to transcardial perfusion with room temperature Sorenson's phosphate buffer (SPB), and fixed with ice-cold 4% paraformaldehyde (PFA) in phosphate buffer (PBS). Brains were removed, trimmed with coronal cuts immediately rostral to the forebrain, post-fixed in 4% PFA for 2 h, cryoprotected in 30% sucrose, embedded in HistoPrep (TM) (SH75–125D, Fisher Chemical) followed by a rapid incubation in −40°C 2-Methylbutane (Fisher Scientific), and kept at −80°C. Fixed brains were cut using the Leica 2800E Frigocut cryostat at −20°C. 35 μm thick free-floating sections were preserved in PBS containing Sodium Azide (0.02%) at 4°C.

Immunofluorescence (free-floating OCT-embedded sections)—The sections were washed in PBS (3 times, 5 minutes each), permeabilized and blocked in a PBS/0.5% Tween 20/1.5% BSA for one hour at room temperature, followed by an overnight incubation with the primary antibody anti-TDP-43 (12892–1-AP, Proteintech; 1:500) diluted in a PBS/0.3%

TritonX100 solution at room temperature. Next, sections were washed in PBS (3 times, 10 minutes each) and incubated with the secondary antibody (diluted in PBS) for one hour, washed twice with PBS (10 minutes each), and then incubated for 10 minutes with PBS/DAPI (Thermo Fisher Scientific, 100ng/ml) solution. Sections were mounted on Fisherbrand Superfrost Plus Microscope Slides (Thermo Fisher Scientific) with ProLong Gold antifade reagent with DAPI (Thermo Fisher Scientific).

Cell culture—All cell lines were cultured at 37 °C in a humidified atmosphere at 5% CO_2. U2OS cells were cultured in DMEM (Gibco) supplemented with 10% fetal bovine serum (FBS) and Antibiotic-Antimycotic (Gibco). SH-SY5Y cells were cultured in DMEM+F12 (Gibco) supplemented with 10% FBS and Antibiotic-Antimycotic. When the cell cycle was arrested in G1, Palbociclib (Apexbio) was added into the media. Cell culture media was changed every 3 days.

Primary hippocampal neuronal cultures were prepared as described previously (Seibenhener and Wooten, 2012) with some modifications. In brief, timed pregnant C57BL/6 mice (Charles River) were sacrificed, and embryos were collected at embryonic day 18 (E18). Primary hippocampal neurons were isolated from both male and female embryos and pooled. Cells were dissociated with 0.125% trypsin, and plated on 96-well glass-bottom plates coated with poly-D-lysine (Sigma-Aldrich) at a cell density of 60,000/ml in neurobasal medium (Gibco) supplemented with 2% B27 (Sigma-Aldrich) and 0.25% glutamine (Sigma-Aldrich). Thereafter, half of the medium was replaced twice a week. Neurons were used 6 to 8 days after plating.

Biochemical fractionation of soluble and insoluble proteins—Cells from six wells were treated as indicated and then lysed in 300 μL of 1x RIPA buffer (50 mM Tris pH 8.0, 150 mM NaCl, 1% NP-40, 5 mM EDTA, 0.5% sodium deoxycholate, 0.1% SDS), supplemented with Halt™ Protease and Phosphatase Inhibitor Cocktail (Thermofisher). After sonication (13% Amp, 5 sec, Branson digital Sonifier), cell lysates were centrifuged at 21,100×g for 30 min at 4°C and the supernatant was collected as the soluble fraction. The pellet fraction was washed with 1x RIPA buffer once before solubilizing in 75 μL of urea buffer (7M urea, 2 M Thiourea, 4% CHAPS, 30 mM Tris, pH 8.5) and cleared by centrifugation at 21,100×g for 30 min at 4°C. Then the soluble and insoluble f ractions were subsequently analysed by western blot.

Immunoblotting—Whole-cell extracts (5×10^6) were directly lysed in SDS sample buffer and boiled for 10 minutes. Samples were resolved by SDS–PAGE, transferred to PVDF, and blocked with 5% milk in TBST (TBS, 0.1% Tween-20). The following primary antibodies were used at 1:1,000 dilution (unless noted) in TBST: anti-TDP-43 (10782–2-AP, Proteintech), anti-tubulin (ab6160, Abcam), anti-GFP (632381, Clontech) and 1:2,000 anti-GAPDH (Ab8245, Abcam), anti-phospho-TDP-43 (829901, Biolegend; 1:500). Blots were probed with 1:5,000 dilutions of HRP-conjugated secondary antibodies (GE Healthcare) and exposed to film.

Live cell imaging—U2OS cells were plated on a density of 8,000 cells per well onto a glass-bottom 96-well plate. TDP-$43^{\Delta NLS\text{-}clover}$ proteins were induced for 24 hours by adding

1μg/mL of doxycycline. TDP-43$^{\Delta NLS\text{-}clover}$ was induced for 48 hours due to the low-level expression of this variant. Live cell imaging was performed on CQ1 Confocal Quantitative Image Cytometer with a 40x objective and environmental control system of 37°C, 95% humid ity and 5% of CO_2. Nine z-stack images (1 μm per stack) were collected per frame, and the maximum intensity projection was used to construct the final image series. To detect the fast fusion behaviour of TDP-43 particles, images were collected at 150 seconds or 30 seconds intervals. For sodium arsenite treatment, 0.25 mM or 50 μM of sodium arsenite was added to the cells and images were collected at 2-min, 5-min or 10-min intervals as indicated. A maximal intensity projection image was generated per frame.

SH-SY5Y TDP-43^{EGFP} cells were plated on 8-well chamber (Ibidi) at 25,000 cells per well. After 24 hours cells were arrested in G1 with Palbociclib (Apexbio) and maintained arrested during the whole length of the experiment. Sonicated fibrils were added at final concentration of 200 nM and media was removed after 3 days. Media was changed every 3 days. Live cell imaging was performed on Olympus FV1000 Spectral Confocal (Olympus) at 60x magnification at environmental control system of 37°C, and 5% of CO_2 at the time points indicated.

Fluorescence recovery after photo bleach (FRAP) analysis—FRAP experiments on U2OS cells were performed on Zeiss LSM880 Aryscan microscope with 40x/1.2 W objective. The intensity of the fluorescent signal is controlled in the detection range through changing the laser power, digital gain and off-set. For the green channel, bleaching was conducted by a 488-nm line from an argon laser at ~80%−100% intensity with ~10–20 iterations. FRAP experiments on SH-SY5Y TDP-43^{EGFP} cells were performed on Olympus FV1000 Spectral Confocal using SIM Scanner with 100x oil immersion objective, bleaching was conducted scanning a region of 1×1 μm for 300ms at 8% of laser intensity at 405-nm. Fluorescence recovery was monitored at 0.5 seconds, 2 seconds, 5 seconds or 10 seconds intervals for 3 minutes. In the focal-bleach experiment roughly half of a particle is bleached or fully photobleached, and then the distribution of the fluorescence within the photo-manipulated particle is determined over time. During the experiment cells were maintained in Leibovitz's L-15 medium (CO_2 independent).

Immunofluorescence from cells—Primary hippocampal neurons, U2OS and SH-SY5Y cells were cultured on 8-well glass-bottom chamber slides (Ibidi). SH-SY5Y cells were plated on 8-well chamber (Ibidi) at 25,000 cells per well. After 24 hours cells were arrested in G1 with Palbociclib (Apexbio) and maintained arrested during the whole length of the experiment. Sonicated fibrils were added at final concentration of 200 nM and media was removed after 3 days. Media was changed every 3 days.

At the indicated time points, cells were fixed with 4% formaldehyde in PBS for 10 minutes at room temperature After two washes with PBS, cells were permeabilized and blocked with blocking solution (0.1% Triton, 2% BSA in PBS) for 1 hour at room temperature. Cells were then incubated overnight with the primary antibody in PBS/0.3% Tween 20. The primary antibodies used for staining were: anti-G3BP1 (ab56574, Abcam; 1:1000), anti-TDP-43 (10782–2-AP, Proteintech; 1:500), anti-TDP-43 (12892–1-AP, Proteintech; 1:500), anti-TIA1 (sc-1751, Santa Cruz; 1:300), anti-HA (mms-101P, Covance; 1:5000), anti-His

(H1029, Sigma; 1:2000), anti-RanGap1 (sc-1862, Santa Cruz; 1:500), anti-Ran (bd-610340, BD Bioscience; 1:500) anti-Nup107 (Ab73290, Abcam; 1:300), anti-Nup62 (MABE1043, Millipore; 1:500), anti-FUS (A303–839A, Bethyl Laboratories; 1:500), anti-phospho-TDP-43 (829901, Biolegend; 1:500), anti-hnRNPA1 (sc-374053, Santa Cruz: 1:500), anti-amyloid A11 (AHB0052, ThermoFisher; 1:500), anti-p62 (GP62-C-WBC, Progen; 1:500), anti-EDC4 (sc-376382, Santa Cruz; 1:100) and anti-MAP2 (NB300–213, Novus Biologicals; 1:500). After three washes with PBS, the cells were subsequently incubated with fluorescently-labelled secondary antibodies diluted at 1:500 in PBS/0.3% Tween 20 for 1 hour at room temperature. After one wash with PBS, one wash with 300 nM DAPWE (PBS) and then one wash with PBS, the cells are preserved in PBS for imaging. SH-SY5Y cells imaging was performed on FV1000 Spectral Confocal (Olympus) at 60–100x magnification.

RNA Fluorescence in situ hybridization (FISH)—All hybridization steps were performed under RNase-free conditions. Cells were fixed in 3.7% formaldehyde for 10 minutes and permeabilized with ethanol 70% for one hour at 4°C. Then, cells were washed with Wash Buffer (1:5 Wash Buffer A, Biosearch techonolgies Cat SMF-WA1–60 plus 1:10 deionized Formamide) and blocked in the dark at 37°C for 4 hours in a humidified chamber with Hybridization Buffer (9:10 RNA FISH Hybridization Buffer Cat SMF-HB1–10 plus 1:10 deionized Formamide) containing 5'-labelled Cy5-(d)T20 oligonucleotides (gift from Dr. J. Paul Taylor, St. Jude Children Hospital) (1ng/μl). After cells were washed with wash buffer in the dark at 37°C for 30 minutes were stai ned with DAPI and proceed to imagining.

SYTO RNA Select Green Fluorescent Cell Stain—All the staining steps were performed under RNase-free conditions. SH-SY5Y cells were fixed with cold methanol at −20°C for 10 minutes and immu nostained with anti-TDP-43 (12892–1-AP, Proteintech; 1:500) following the protocol described. Then, cells were washed with PBS two times and stained with freshly prepared RNASelect (Molecular Probes) (500 nM) at room temperature for 20 minutes. Finally, cells were washed for 5 minutes in PBS and stained with DAPI.

Recombinant protein purification—All proteins were expressed and purified from *E. colwe* BL21 under native conditions. Protein expression was induced with 1 mM IPTG for 16 hours at 16°C. *E.colwe* cells were lysed by sonication on ice in PBS with protease inhibitors (cOmplete, EDTA-free, Roche Applied Science). HA-FUS expression constructs were generated in pGST-Duet to contain a TEV-cleavable site, resulting in GST-TEV-HA-FUS construct. The protein was purified over pre-packed Glutathione Sepharose High Performance resin (GSTrap HP columns, GE) with one-step purification of glutathione S-Transferase (GST) tagged FUS protein using Akta Pure fast protein liquid chromatography (FPLC) system (GE) at 4°C. GST-HA-FUS protein was eluted in mM Tris-HCl, pH 8, 200 mM trehalose, and 20 mM glutathione. His-TDP-43 WT, His-TDP-43$^{WT\text{-}mCherry}$, His-TDP-43$^{G298S\text{-}mCherry}$, His-SOD1$^{WT\text{-}mCherry}$ and His-FUS$^{WT\text{-}mCherry}$ proteins were purified over pre-packed Nwe Sepharose High Performance HisTrap HP (GE) using an AKTA pure chromatography system at 4°C and eluted with 5 0 mM Tris pH 7.4, 100 mM NaCl and 400 mM Imidazole. In the case of His-TDP-43$^{WT\text{-}mCherry}$ Ni-IMAC eluted fractions were followed by gel Filtration Chromatography (Superdex 75 10/300, GE). The following

Molecular Weight Markers were used: Carbonic Anhydrase from bovine erythrocytes (29 KDa, Sigma), Albumin, bovine serum (66KDa, Sigma) and β-Amylase from sweet potato, (200KDa, Sigma). Eluted proteins (GST-HA-FUS, His-TDP-43$^{G298S\text{-}mCherry}$, His-SOD1$^{WT\text{-}mCherry}$ and His-FUS$^{WT\text{-}mCherry}$) with the expected size were collected and concentrated to final concentration of 12 μM using Amicon Ultra centrifugal filter units (10 kDa molecular weight cut-off; Millipore). All proteins after purification were centrifuged for 15 minutes at 14,000 rpm at 4°C to remove any aggregated material. Protein concentration was calculated by Coomassie Blue with BSA protein as standard, and by colorimetric Bradford assay (Bio-Rad). For protein storage at −80°C glycerol was added (30%)

Amyloid-fibrils reconstruction—HA-FUS^{WT} protein was buffer exchanged at 4°C into FUS assem bly buffer (50 mM Tris-HCl, pH 8, 200 mM trehalose, 1 mM DTT, 20 mM glutathione). Seed formation was initiated by addition of TEV protease to GST-TEV-HA-FUS (4 μM) in FUS assembly buffer for 3 hours and then high salt storage buffer (40 mM HEPES pH7.4, 500 mM KCl, 20 mM MgCl2, 10% glycerol, 1 mM DTT) was added for 3 hours (Sun et al., 2011). FUS fibrilization was initiated by adding 1:20 of FUS seeds to GST-TEV-FUS (4 μM) and TEV protease in FUS assembly buffer for 24 hours at 22°C. The fibrils generated were sonicated at 45% f or 45 seconds. Sonicated fibrils were used as seeds on the following FUS fibrilization assays. His-FUS^{mCherry} was initially dialyzed with FUS$^{WT\text{-}mCherry}$ assembly buffer (Tris 50 mM pH 7.4, 100 mM NaCl, 1 mM DTT). Fibrils were generated by adding sonicated HA-FUS^{WT} fibrils to His-FUS$^{WT\text{-}mCherry}$ (4 μM) for 24 hours at 22°C.

His-TDP-43 protein (4 μM) was initially dialyzed at 4°C with Tris 50 mM pH 7.4, 100 mM NaCl, 1 mM DTT buffer. Fibrils were induced by adding polyethylene glycol (PEG)-4000 (7%) and 2-methyl-2,4-pentanediol (MPD) (3%) for 16 hours at 22°C. Sonicated His-TDP-43 fibrils were used as seeds on the following TDP-43 fibrilization assays. His-TDP-43$^{WT\text{-}mCherry}$ fibrils were generated by adding sonicated His-TDP-43 fibrils as seeds to soluble His-TDP-43$^{WT\text{-}mCherry}$ in TDP-43 assembly buffer supplemented with 7% PEG and 3% MPD.

His-SOD1$^{G93A\text{-}mCherry}$ fibrilization was induced by adding SOD1^{A4V} aggregates produced in bacteria. Briefly, SOD1^{A4V} protein aggregates were induced in BL21 cells, bacteria cell pellet was collected, lysed and centrifuged/resuspended for 5 cycles (Molina-Garcia et al., 2018). Then a sucrose discontinuous gradient was prepared: in a 2 ml Eppendorf tube, successively was displayed 200 μl of 60 (bottom)> 50 > 40 > 30 > 20% (top) sucrose, freezing each layer at − 80°C before adding the next one. Resuspended aggreg ates were laid on the sucrose gradient and centrifuged at 10,000 rpm 1 hour at 4°C. Fracti ons were carefully collected and a Coomassie Blue gel was performed to identify the fraction(s) that contained SOD1^{A4V} protein. SOD1^{A4V} containing fractions were further dialyzed with PBS and sonicated. The final product was used as seeds for His-SOD1$^{G93A\text{-}mCherry}$ fibrilization. Seeds were added to His-SOD1$^{G93A\text{-}mCherry}$ (4 μM) in SOD1 assembly buffer (100 mM Na_2SO_4, 30 mM Tris–HCl pH 8, 4 mM $MgSO_4$, 7% polyethylene glycol (PEG)-4000 and 3% 2-methyl-2,4-pentanediol (MPD)) at 22°C during 16 hours. Finally, fibrils were dialyzed using slide-A-Lyzer MINWE Dialysis Units (10 kDa molecular weight cut-off; Thermo) in PBS for 3 hours and sonicated at 45% 45 seconds just before adding them to the cell media.

Transmission Electron Microscopy—Fibril protein reactions (10 μl) were adsorbed onto glow-discharged 300-mesh Formvar/carbon coated copper grids (Ted Pella) and stained with 2% (w/v) aqueous uranyl acetate (Ladd Research Industries, Williston, VT). Excess liquid was removed, and grids were allowed to air dry. Grids were examined using a Tecnawe G2 Spirit BioTWIN transmission electron microscope equipped with an Eagle 4k HS digital camera (FEI, Hilsboro, OR).

Survival curve—For survival curve analysis, SH-SY5Y TDP-43^{EGFP} cells were plated on a 24 well-plate and cytoplasmic LLPS were induced with His-FUS^{mCherry} fibrils as described. At indicated time points, cells were collected and counted using a haemocytometer (Fisher Scientific).

QUANTIFICATION AND STATISTICAL ANALYSIS

All quantitative analyses relied on systematic uniform random sampling.

1. **FRAP—**The FRAP data was quantified using Image J. The time series of the granule fluorescence intensity was calculated and the intensity of the background (area with no cells) was subtracted from the granule intensity. The intensity of the granule during the whole experiment was normalized to one before bleaching and the intensity of the granule just after bleaching was normalized to zero. An average of at least 4–20 particles per condition was used to calculate the mean and standard deviation. The averaged relative intensity and standard error were plotted to calculate the dynamics of the particles.

2. **Cytoplasmic TDP-43 LLPS—**Number of cells with cytoplasmic TDP-43 particles and number of cytoplasmic particles were counted on 60x images taken on the Olympus FV1000 Spectral Confocal. DAPI staining was used to address cytoplasmic localization. ~200 cells were counted per condition and time point. Quantification was performed in at least three independent replicates. Arsenite induced cytoplasmic TDP-43 demixing was done using live cell imaging on CQ1 Confocal Quantitative Image Cytometer with a 40x objective and environmental control system of 37°C, 95% humidity and 5% of CO_2. Quantification of the cells was done on five independent videos at the corresponding time point with a total number of 93 cells.

3. **Fluorescence quantification of Clover in living cells—**U2OS were plated on 8-well glass-bottom chamber slides (Ibidi). Imaging of TDP-43$^{\Delta NLS\text{-}clover}$ were done using the 20x objective (0.8. air. 0.55 mm) on Zeiss LSM880 confocal microscope with settings: scan resolution = 1024 × 1024; scan speed level = 8; pinhole = 20; Gain was set at 500 and offset was set to 600 to allow all the signal in the picture is in linear range. 488 nm were used for excitation and the signals from 500 nm to 600 nm were collected. Mean intensity of TDP-43$^{\Delta NLS\text{-}clover}$ in the cytoplasm was measured using FIJI (ImageJ) by circling the area of the cells with fluorescence. Dot plotting of the intensity from 23 cells with TDP-43 granules, and 27 cells without granules from nine images.

4. **Cell survival and TDP-43 LLPS with nuclear depletion—**Cell survival was quantified manually with using a haemocytometer. The number of survival cells was

normalized to day 1 post-fibrils treatment. Non-fibrils treated cells were added as control. Survival was measured in at least three independent replicates.

Quantifications of the percentage of cells with cytoplasmic LLPS (with or without nuclear TDP-43 clearance), or with cytoplasmic LLPS accompanied by nuclear clearance were quantified manually on 60x images taken on the Olympus FV1000 Spectral Confocal. DAPI staining was used to address cytoplasmic localization. Data are represented as mean ± SEM from a total of three independent experiments.

5. **RanGap1 aggregates—**Number of cells with cytoplasmic RanGap1 aggregates were counted manually on 60x images taken on the Olympus FV1000 Spectral Confocal. 200 cells were counted. Quantification was performed in at least three independent replicates.

Statistical Analysis: Statistical analyses were performed using GraphPad Prism. All data are shown as the box whisker plot (mean, min and max value) or mean ± standard error of the mean (SEM). The statistical significance of the differences between two groups was investigated by paired t test. Statistical tests are indicated in each figure legend along with the corresponding significance level (p value). The number of cells analyzed per experiment is provided in the corresponding figure legends.

Supplementary Material

Refer to Web version on PubMed Central for supplementary material.

Acknowledgments

We would like to thank Mrs. Jennifer Santini (UCSD, Light Microscopy Core) and Mr. Timo Merlo (UCSD, Electron Microscopy Core) for resources. We thank iXCells Biotechnologies for providing human iPSC-derived motor neuron precursor cells. This work was supported by grants from the NIH (R01-NS27036 and P40-NS047101) and the Nomis Foundation. F.G.-R is the recipient of career development awards from the Muscular Dystrophy Association and Target ALS. H.Y. is recipient of a postdoctoral fellowship from the NIH (F32-AG059358). C.C. received salary support from the ALS Association. Z.M was recipient of a Human Frontiers Science Program (HFSP) long-term fellowship. D.W.C. and S.D.C. receive salary support from the Ludwig Institute for Cancer Research.

LITERATURE CITED

Afroz T, Hock EM, Ernst P, Foglieni C, Jambeau M, Gilhespy LAB, Laferriere F, Maniecka Z, Pluckthun A, Mittl P, et al. (2017). Functional and dynamic polymerization of the ALS-linked protein TDP-43 antagonizes its pathologic aggregation. Nat Commun 8, 45. [PubMed: 28663553]

Ayala YM, De Conti L, Avendano-Vazquez SE, Dhir A, Romano M, D'Ambrogio A, Tollervey J, Ule J, Baralle M, Buratti E, et al. (2011). TDP-43 regulates its mRNA levels through a negative feedback loop. EMBO J 30, 277–288. [PubMed: 21131904]

Ayala YM, Zago P, D'Ambrogio A, Xu YF, Petrucelli L, Buratti E, and Baralle FE (2008). Structural determinants of the cellular localization and shuttling of TDP-43. J Cell Sci 121, 3778–3785. [PubMed: 18957508]

Becker LA, Huang B, Bieri G, Ma R, Knowles DA, Jafar-Nejad P, Messing J, Kim HJ, Soriano A, Auburger G, et al. (2017). Therapeutic reduction of ataxin-2 extends lifespan and reduces pathology in TDP-43 mice. Nature 544, 367–371. [PubMed: 28405022]

Boeynaems S, Alberti S, Fawzi NL, Mittag T, Polymenidou M, Rousseau F, Schymkowitz J, Shorter J, Wolozin B, Van Den Bosch L, et al. (2018). Protein Phase Separation: A New Phase in Cell Biology. Trends Cell Biol

Boeynaems S, Bogaert E, Van Damme P, and Van Den Bosch L (2016). Inside out: the role of nucleocytoplasmic transport in ALS and FTLD. Acta Neuropathol 132, 159–173. [PubMed: 27271576]

Brady OA, Meng P, Zheng Y, Mao Y, and Hu F (2011). Regulation of TDP-43 aggregation by phosphorylation and p62/SQSTM1. J Neurochem 116, 248–259. [PubMed: 21062285]

Brangwynne CP, Eckmann CR, Courson DS, Rybarska A, Hoege C, Gharakhani J, Julicher F, and Hyman AA (2009). Germline P granules are liquid droplets that localize by controlled dissolution/condensation. Science 324, 1729–1732. [PubMed: 19460965]

Burke KA, Janke AM, Rhine CL, and Fawzi NL (2015). Residue-by-Residue View of In Vitro FUS Granules that Bind the C-Terminal Domain of RNA Polymerase II. Mol Cell 60, 231–241. [PubMed: 26455390]

Chiti F, and Dobson CM (2006). Protein misfolding, functional amyloid, and human disease. Annu Rev Biochem 75, 333–366. [PubMed: 16756495]

Chou CC, Zhang Y, Umoh ME, Vaughan SW, Lorenzini I, Liu F, Sayegh M, Donlin-Asp PG, Chen YH, Duong DM, et al. (2018). TDP-43 pathology disrupts nuclear pore complexes and nucleocytoplasmic transport in ALS/FTD. Nat Neurosci 21, 228–239. [PubMed: 29311743]

Colombrita C, Zennaro E, Fallini C, Weber M, Sommacal A, Buratti E, Silani V, and Ratti A (2009). TDP-43 is recruited to stress granules in conditions of oxidative insult. J Neurochem 111, 1051–1061. [PubMed: 19765185]

Cong L, Ran FA, Cox D, Lin S, Barretto R, Habib N, Hsu PD, Wu X, Jiang W, Marraffini LA, et al. (2013). Multiplex genome engineering using CRISPR/Cas systems. Science 339, 819–823. [PubMed: 23287718]

Conicella AE, Zerze GH, Mittal J, and Fawzi NL (2016). ALS Mutations Disrupt Phase Separation Mediated by alpha-Helical Structure in the TDP-43 Low-Complexity C-Terminal Domain. Structure 24, 1537–1549. [PubMed: 27545621]

Coyne AN, Yamada SB, Siddegowda BB, Estes PS, Zaepfel BL, Johannesmeyer JS, Lockwood DB, Pham LT, Hart MP, Cassel JA, et al. (2015). Fragile X protein mitigates TDP-43 toxicity by remodeling RNA granules and restoring translation. Hum Mol Genet 24, 6886–6898. [PubMed: 26385636]

D'Angelo MA, Raices M, Panowski SH, and Hetzer MW (2009). Age-dependent deterioration of nuclear pore complexes causes a loss of nuclear integrity in postmitotic cells. Cell 136, 284–295. [PubMed: 19167330]

Dao TP, Kolaitis RM, Kim HJ, O'Donovan K, Martyniak B, Colicino E, Hehnly H, Taylor JP, and Castaneda CA (2018). Ubiquitin Modulates Liquid-Liquid Phase Separation of UBQLN2 via Disruption of Multivalent Interactions. Mol Cell 69, 965–978 e966. [PubMed: 29526694]

Ditsworth D, Maldonado M, McAlonis-Downes M, Sun S, Seelman A, Drenner K, Arnold E, Ling SC, Pizzo D, Ravits J, et al. (2017). Mutant TDP-43 within motor neurons drives disease onset but not progression in amyotrophic lateral sclerosis. Acta Neuropathol 133, 907–922. [PubMed: 28357566]

Dormann D, Rodde R, Edbauer D, Bentmann E, Fischer I, Hruscha A, Than ME, Mackenzie IR, Capell A, Schmid B, et al. (2010). ALS-associated fused in sarcoma (FUS) mutations disrupt Transportin-mediated nuclear import. EMBO J 29, 2841–2857. [PubMed: 20606625]

Elden AC, Kim HJ, Hart MP, Chen-Plotkin AS, Johnson BS, Fang X, Armakola M, Geser F, Greene R, Lu MM, et al. (2010). Ataxin-2 intermediate-length polyglutamine expansions are associated with increased risk for ALS. Nature 466, 1069–1075. [PubMed: 20740007]

Freibaum BD, Lu Y, Lopez-Gonzalez R, Kim NC, Almeida S, Lee KH, Badders N, Valentine M, Miller BL, Wong PC, et al. (2015). GGGGCC repeat expansion in C9orf72 compromises nucleocytoplasmic transport. Nature 525, 129–133. [PubMed: 26308899]

Fuentealba RA, Udan M, Bell S, Wegorzewska I, Shao J, Diamond MI, Weihl CC, and Baloh RH (2010). Interaction with polyglutamine aggregates reveals a Q/N-rich domain in TDP-43. J Biol Chem 285, 26304–26314. [PubMed: 20554523]

Gasset-Rosa F, Chillon-Marinas C, Goginashvili A, Atwal RS, Artates JW, Tabet R, Wheeler VC, Bang AG, Cleveland DW, and Lagier-Tourenne C (2017). Polyglutamine-Expanded Huntingtin

Exacerbates Age-Related Disruption of Nuclear Integrity and Nucleocytoplasmic Transport. Neuron 94, 48–57 e44. [PubMed: 28384474]

Gopal PP, Nirschl JJ, Klinman E, and Holzbaur EL (2017). Amyotrophic lateral sclerosis-linked mutations increase the viscosity of liquid-like TDP-43 RNP granules in neurons. Proc Natl Acad Sci U S A 114, E2466–E2475. [PubMed: 28265061]

Guo L, Kim HJ, Wang H, Monaghan J, Freyermuth F, Sung JC, O'Donovan K, Fare CM, Diaz Z, Singh N, et al. (2018). Nuclear-Import Receptors Reverse Aberrant Phase Transitions of RNA-Binding Proteins with Prion-like Domains. Cell 173, 677–692 e620. [PubMed: 29677512]

Hofweber M, Hutten S, Bourgeois B, Spreitzer E, Niedner-Boblenz A, Schifferer M, Ruepp MD, Simons M, Niessing D, Madl T, et al. (2018). Phase Separation of FUS Is Suppressed by Its Nuclear Import Receptor and Arginine Methylation. Cell 173, 706–719 e713. [PubMed: 29677514]

Jain S, Ba Z, Zhang Y, Dai HQ, and Alt FW (2018). CTCF-Binding Elements Mediate Accessibility of RAG Substrates During Chromatin Scanning. Cell 174, 102–116 e114. [PubMed: 29804837]

Jakel S, Mingot JM, Schwarzmaier P, Hartmann E, and Gorlich D (2002). Importins fulfil a dual function as nuclear import receptors and cytoplasmic chaperones for exposed basic domains. EMBO J 21, 377–386. [PubMed: 11823430]

Johnson BS, Snead D, Lee JJ, McCaffery JM, Shorter J, and Gitler AD (2009). TDP-43 is intrinsically aggregation-prone, and amyotrophic lateral sclerosis-linked mutations accelerate aggregation and increase toxicity. J Biol Chem 284, 20329–20339. [PubMed: 19465477]

Jovicic A, Mertens J, Boeynaems S, Bogaert E, Chai N, Yamada SB, Paul JW 3rd, Sun S, Herdy JR, Bieri G, et al. (2015). Modifiers of C9orf72 dipeptide repeat toxicity connect nucleocytoplasmic transport defects to FTD/ALS. Nat Neurosci 18, 1226–1229. [PubMed: 26308983]

Kayed R, Head E, Sarsoza F, Saing T, Cotman CW, Necula M, Margol L, Wu J, Breydo L, Thompson JL, et al. (2007). Fibril specific, conformation dependent antibodies recognize a generic epitope common to amyloid fibrils and fibrillar oligomers that is absent in prefibrillar oligomers. Mol Neurodegener 2, 18. [PubMed: 17897471]

Khalfallah Y, Kuta R, Grasmuck C, Prat A, Durham HD, and Vande Velde C (2018). TDP-43 regulation of stress granule dynamics in neurodegenerative disease-relevant cell types. Sci Rep 8, 7551. [PubMed: 29765078]

King OD, Gitler AD, and Shorter J (2012). The tip of the iceberg: RNA-binding proteins with prion-like domains in neurodegenerative disease. Brain Res 1462, 61–80. [PubMed: 22445064]

Kinoshita Y, Ito H, Hirano A, Fujita K, Wate R, Nakamura M, Kaneko S, Nakano S, and Kusaka H (2009). Nuclear contour irregularity and abnormal transporter protein distribution in anterior horn cells in amyotrophic lateral sclerosis. Journal of neuropathology and experimental neurology 68, 1184–1192. [PubMed: 19816199]

Laferriere F, Maniecka Z, Perez-Berlanga M, Hruska-Plochan M, Gilhespy L, Hock EM, Wagner U, Afroz T, Boersema PJ, Barmettler G, et al. (2019). TDP-43 extracted from frontotemporal lobar degeneration subject brains displays distinct aggregate assemblies and neurotoxic effects reflecting disease progression rates. Nat Neurosci 22, 65–77. [PubMed: 30559480]

Li P, Banjade S, Cheng HC, Kim S, Chen B, Guo L, Llaguno M, Hollingsworth JV, King DS, Banani SF, et al. (2012). Phase transitions in the assembly of multivalent signalling proteins. Nature 483, 336–340. [PubMed: 22398450]

Li YR, King OD, Shorter J, and Gitler AD (2013). Stress granules as crucibles of ALS pathogenesis. J Cell Biol 201, 361–372. [PubMed: 23629963]

Ling SC, Polymenidou M, and Cleveland DW (2013). Converging mechanisms in ALS and FTD: disrupted RNA and protein homeostasis. Neuron 79, 416–438. [PubMed: 23931993]

Liu-Yesucevitz L, Bilgutay A, Zhang YJ, Vanderweyde T, Citro A, Mehta T, Zaarur N, McKee A, Bowser R, Sherman M, et al. (2010). Tar DNA binding protein-43 (TDP-43) associates with stress granules: analysis of cultured cells and pathological brain tissue. PLoS One 5, e13250. [PubMed: 20948999]

Mackenzie IR, Nicholson AM, Sarkar M, Messing J, Purice MD, Pottier C, Annu K, Baker M, Perkerson RB, Kurti A, et al. (2017). TIA1 Mutations in Amyotrophic Lateral Sclerosis and

Frontotemporal Dementia Promote Phase Separation and Alter Stress Granule Dynamics. Neuron 95, 808–816 e809. [PubMed: 28817800]

Maharana S, Wang J, Papadopoulos DK, Richter D, Pozniakovsky A, Poser I, Bickle M, Rizk S, Guillen-Boixet J, Franzmann T, et al. (2018). RNA buffers the phase separation behavior of prion-like RNA binding proteins. Science

Malinovska L, Kroschwald S, and Alberti S (2013). Protein disorder, prion propensities, and self-organizing macromolecular collectives. Biochim Biophys Acta 1834, 918–931. [PubMed: 23328411]

Markmiller S, Soltanieh S, Server KL, Mak R, Jin W, Fang MY, Luo EC, Krach F, Yang D, Sen A, et al. (2018). Context-Dependent and Disease-Specific Diversity in Protein Interactions within Stress Granules. Cell 172, 590–604 e513. [PubMed: 29373831]

Marrone L, Poser I, Casci I, Japtok J, Reinhardt P, Janosch A, Andree C, Lee HO, Moebius C, Koerner E, et al. (2018). Isogenic FUS-eGFP iPSC Reporter Lines Enable Quantification of FUS Stress Granule Pathology that Is Rescued by Drugs Inducing Autophagy. Stem Cell Reports 10, 375–389. [PubMed: 29358088]

Mateju D, Franzmann TM, Patel A, Kopach A, Boczek EE, Maharana S, Lee HO, Carra S, Hyman AA, and Alberti S (2017). An aberrant phase transition of stress granules triggered by misfolded protein and prevented by chaperone function. EMBO J 36, 1669–1687. [PubMed: 28377462]

McGurk L, Gomes E, Guo L, Mojsilovic-Petrovic J, Tran V, Kalb RG, Shorter J, and Bonini NM (2018). Poly(ADP-Ribose) Prevents Pathological Phase Separation of TDP-43 by Promoting Liquid Demixing and Stress Granule Localization. Mol Cell 71, 703–717 e709. [PubMed: 30100264]

McGurk L, Lee VM, Trojanowksi JQ, Van Deerlin VM, Lee EB, and Bonini NM (2014). Poly-A binding protein-1 localization to a subset of TDP-43 inclusions in amyotrophic lateral sclerosis occurs more frequently in patients harboring an expansion in C9orf72. J Neuropathol Exp Neurol 73, 837–845. [PubMed: 25111021]

Melamed Z, Lopez-Erauskin J, Baughn MW, Zhang O, Drenner K, Sun Y, Freyermuth F, McMahon MA, Beccari MS, Artates JW, et al. (2019). Premature polyadenylation-mediated loss of stathmin-2 is a hallmark of TDP-43-dependent neurodegeneration. Nat Neurosci 22, 180–190. [PubMed: 30643298]

Mertens J, Paquola AC, Ku M, Hatch E, Bohnke L, Ladjevardi S, McGrath S, Campbell B, Lee H, Herdy JR, et al. (2015). Directly Reprogrammed Human Neurons Retain Aging-Associated Transcriptomic Signatures and Reveal Age-Related Nucleocytoplasmic Defects. Cell Stem Cell 17, 705–718. [PubMed: 26456686]

Mitrea DM, and Kriwacki RW (2016). Phase separation in biology; functional organization of a higher order. Cell Commun Signal 14, 1. [PubMed: 26727894]

Molina-Garcia L, Gasset-Rosa F, Alamo MM, de la Espina SM, and Giraldo R (2018). Addressing Intracellular Amyloidosis in Bacteria with RepA-WH1, a Prion-Like Protein. Methods Mol Biol 1779, 289–312. [PubMed: 29886540]

Molliex A, Temirov J, Lee J, Coughlin M, Kanagaraj AP, Kim HJ, Mittag T, and Taylor JP (2015). Phase Separation by Low Complexity Domains Promotes Stress Granule Assembly and Drives Pathological Fibrillization. Cell 163, 123–133. [PubMed: 26406374]

Neumann M, Igaz LM, Kwong LK, Nakashima-Yasuda H, Kolb SJ, Dreyfuss G, Kretzschmar HA, Trojanowski JQ, and Lee VM (2007). Absence of heterogeneous nuclear ribonucleoproteins and survival motor neuron protein in TDP-43 positive inclusions in frontotemporal lobar degeneration. Acta Neuropathol 113, 543–548. [PubMed: 17415574]

Neumann M, Sampathu DM, Kwong LK, Truax AC, Micsenyi MC, Chou TT, Bruce J, Schuck T, Grossman M, Clark CM, et al. (2006). Ubiquitinated TDP-43 in frontotemporal lobar degeneration and amyotrophic lateral sclerosis. Science 314, 130–133. [PubMed: 17023659]

Patel A, Lee HO, Jawerth L, Maharana S, Jahnel M, Hein MY, Stoynov S, Mahamid J, Saha S, Franzmann TM, et al. (2015). A Liquid-to-Solid Phase Transition of the ALS Protein FUS Accelerated by Disease Mutation. Cell 162, 1066–1077. [PubMed: 26317470]

Polymenidou M, Lagier-Tourenne C, Hutt KR, Huelga SC, Moran J, Liang TY, Ling SC, Sun E, Wancewicz E, Mazur C, et al. (2011). Long pre-mRNA depletion and RNA missplicing contribute to neuronal vulnerability from loss of TDP-43. Nat Neurosci 14, 459–468. [PubMed: 21358643]

Qamar S, Wang G, Randle SJ, Ruggeri FS, Varela JA, Lin JQ, Phillips EC, Miyashita A, Williams D, Strohl F, et al. (2018). FUS Phase Separation Is Modulated by a Molecular Chaperone and Methylation of Arginine Cation-pi Interactions. Cell 173, 720–734 e715. [PubMed: 29677515]

Ramaswami M, Taylor JP, and Parker R (2013). Altered ribostasis: RNA-protein granules in degenerative disorders. Cell 154, 727–736. [PubMed: 23953108]

Rambaran RN, and Serpell LC (2008). Amyloid fibrils: abnormal protein assembly. Prion 2, 112–117. [PubMed: 19158505]

Rutherford NJ, Zhang YJ, Baker M, Gass JM, Finch NA, Xu YF, Stewart H, Kelley BJ, Kuntz K, Crook RJ, et al. (2008). Novel mutations in TARDBP (TDP-43) in patients with familial amyotrophic lateral sclerosis. PLoS genetics 4, e1000193. [PubMed: 18802454]

Ryan VH, Dignon GL, Zerze GH, Chabata CV, Silva R, Conicella AE, Amaya J, Burke KA, Mittal J, and Fawzi NL (2018). Mechanistic View of hnRNPA2 Low-Complexity Domain Structure, Interactions, and Phase Separation Altered by Mutation and Arginine Methylation. Mol Cell 69, 465–479 e467. [PubMed: 29358076]

Scaffidi P, and Misteli T (2006). Lamin A-dependent nuclear defects in human aging. Science 312, 1059–1063. [PubMed: 16645051]

Seibenhener ML, and Wooten MW (2012). Isolation and culture of hippocampal neurons from prenatal mice. J Vis Exp

Sreedharan J, Blair IP, Tripathi VB, Hu X, Vance C, Rogelj B, Ackerley S, Durnall JC, Williams KL, Buratti E, et al. (2008). TDP-43 mutations in familial and sporadic amyotrophic lateral sclerosis. Science 319, 1668–1672. [PubMed: 18309045]

Sun Z, Diaz Z, Fang X, Hart MP, Chesi A, Shorter J, and Gitler AD (2011). Molecular determinants and genetic modifiers of aggregation and toxicity for the ALS disease protein FUS/TLS. PLoS biology 9, e1000614. [PubMed: 21541367]

Taylor JP, Brown RH Jr., and Cleveland DW (2016). Decoding ALS: from genes to mechanism. Nature 539, 197–206. [PubMed: 27830784]

Tollervey JR, Curk T, Rogelj B, Briese M, Cereda M, Kayikci M, Konig J, Hortobagyi T, Nishimura AL, Zupunski V, et al. (2011). Characterizing the RNA targets and position-dependent splicing regulation by TDP-43. Nat Neurosci 14, 452–458. [PubMed: 21358640]

Vogler TO, Wheeler JR, Nguyen ED, Hughes MP, Britson KA, Lester E, Rao B, Betta ND, Whitney ON, Ewachiw TE, et al. (2018). TDP-43 and RNA form amyloid-like myo-granules in regenerating muscle. Nature 563, 508–513. [PubMed: 30464263]

Wang A, Conicella AE, Schmidt HB, Martin EW, Rhoads SN, Reeb AN, Nourse A, Ramirez Montero D, Ryan VH, Rohatgi R, et al. (2018). A single N-terminal phosphomimic disrupts TDP-43 polymerization, phase separation, and RNA splicing. EMBO J 37.

Yoshizawa T, Ali R, Jiou J, Fung HYJ, Burke KA, Kim SJ, Lin Y, Peeples WB, Saltzberg D, Soniat M, et al. (2018). Nuclear Import Receptor Inhibits Phase Separation of FUS through Binding to Multiple Sites. Cell 173, 693–705 e622. [PubMed: 29677513]

Zhang J, Ito H, Wate R, Ohnishi S, Nakano S, and Kusaka H (2006). Altered distributions of nucleocytoplasmic transport-related proteins in the spinal cord of a mouse model of amyotrophic lateral sclerosis. Acta Neuropathol 112, 673–680. [PubMed: 16957927]

Zhang K, Daigle JG, Cunningham KM, Coyne AN, Ruan K, Grima JC, Bowen KE, Wadhwa H, Yang P, Rigo F, et al. (2018). Stress Granule Assembly Disrupts Nucleocytoplasmic Transport. Cell 173, 958–971 e917. [PubMed: 29628143]

Zhang K, Donnelly CJ, Haeusler AR, Grima JC, Machamer JB, Steinwald P, Daley EL, Miller SJ, Cunningham KM, Vidensky S, et al. (2015). The C9orf72 repeat expansion disrupts nucleocytoplasmic transport. Nature 525, 56–61. [PubMed: 26308891]

Highlights

- Transient stress induces long-lasting phase separation of cytoplasmic TDP-43
- Formation/maintenance of phase separated TDP-43 is independent of stress granules
- Phase separated TDP-43 inhibits nuclear transport by demixing importin-α and Nup62
- Cytoplasmic TDP-43 demixing depletes nuclear TDP-43 and induces cell death

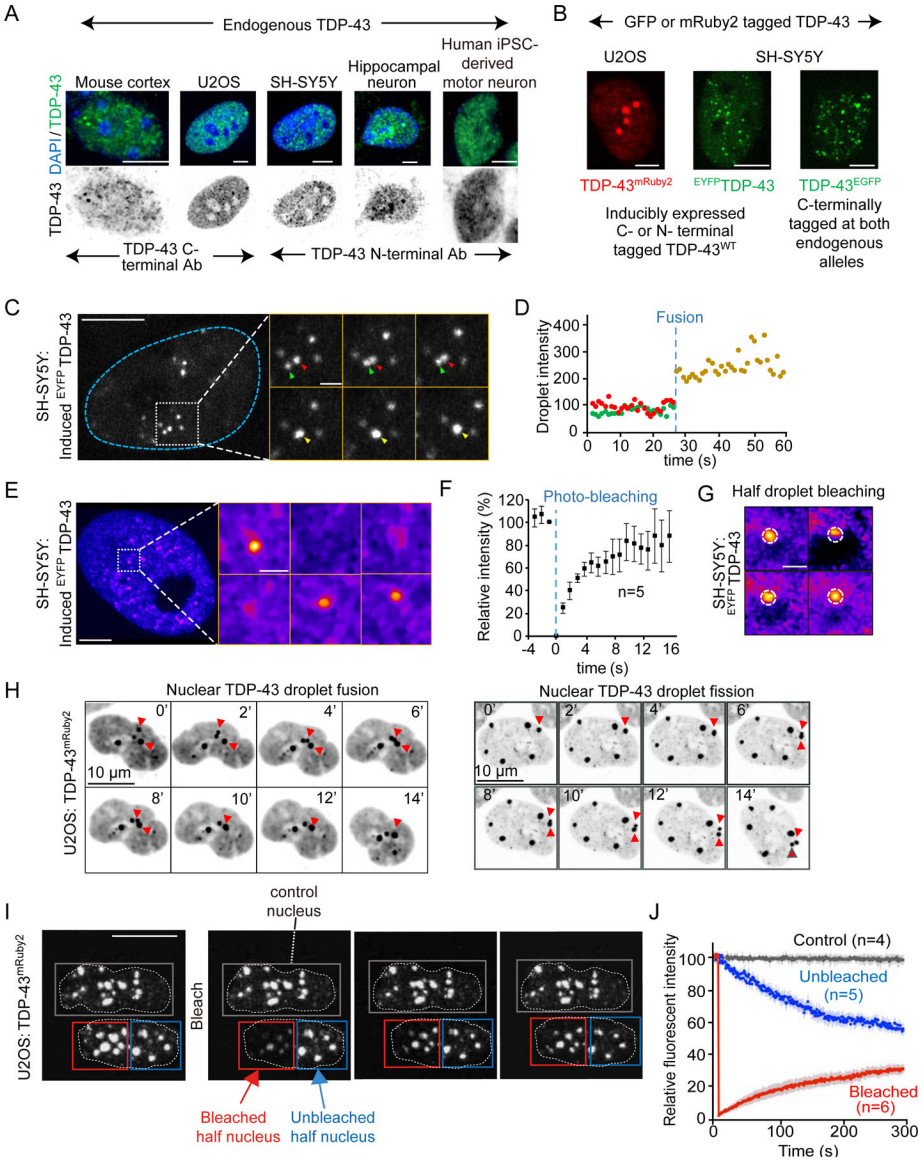

Figure 1. Nuclear TDP-43 de-mixes under physiological conditions.

(A) Endogenous TDP-43 detected by immunofluorescence (green) in multiple cell types (upper panels). Endogenous TDP-43 (green) and DAPI (blue); (lower panels) TDP-43 only (inverted in gray). (B) Representative images of nuclear particles of full-length TDP-43 in U2OS or SH-SY5Y cells stably expressing wild-type TDP-43 C-terminally tagged with mRuby2 (TDP-43^{mRuby2}; left) or N-terminally tagged with EYFP (^{EYFP}TDP-43; middle), respectively. C-terminally EGFP tagged TDP-43 expressed from both endogenous alleles in SH-SY5Y (right panel). (C) Representative fusion event of nuclear ^{EYFP}TDP-43 droplets in SH-SY5Y cells 24 hours post-induction of ^{EYFP}TDP-43 expression. Higher magnification is shown in the right panels. The green and red arrowheads point to two separated droplets before fusion, while the yellow one points to the fused droplet. (D) Fluorescence intensity of the indicated droplets in (C) before (red and green arrowheads) and after (yellow arrowhead) fusion, normalized to average droplet intensity before fusion. (E) FRAP of ^{EYFP}TDP-43

droplets in SH-SY5Y cells after 24 hours of expression. Higher magnification is shown in the right panel. The whole droplet was photobleached at 0''. (F) Mean fluorescence intensity at the bleached area shown in (E) plotted over time, normalized to the average intensity of a droplet before photobleaching and represented as mean ± SEM [from the recovery curves of 5 droplets in a total of three independent experiments]. (G) FRAP of partial photobleaching of ^{EYFP}TDP-43 droplets in SH-SY5Y cells 24 hours after ^{EYFP}TDP-43 induction. (H) Fusion and fission events of TDP-43^{mRuby2} droplets in U2OS cells. Red arrowheads point to fusing or dividing droplets. (I) FRAP of nuclear TDP-43^{mRuby2} in U2OS cells. Half of one nucleus (outlined by the red box) was photobleached at 0''. The blue box outlines the unbleached area of the other half of the nucleus; the gray box outlines an unbleached control nucleus in an adjacent cell. (J) Mean fluorescence intensity (normalized to the unbleached control nucleus) in the bleached and unbleached areas shown in plotted over time (represented as mean ± SEM from the recovery curves of 3 nuclei in a total of three independent experiments). See also Figure S1.

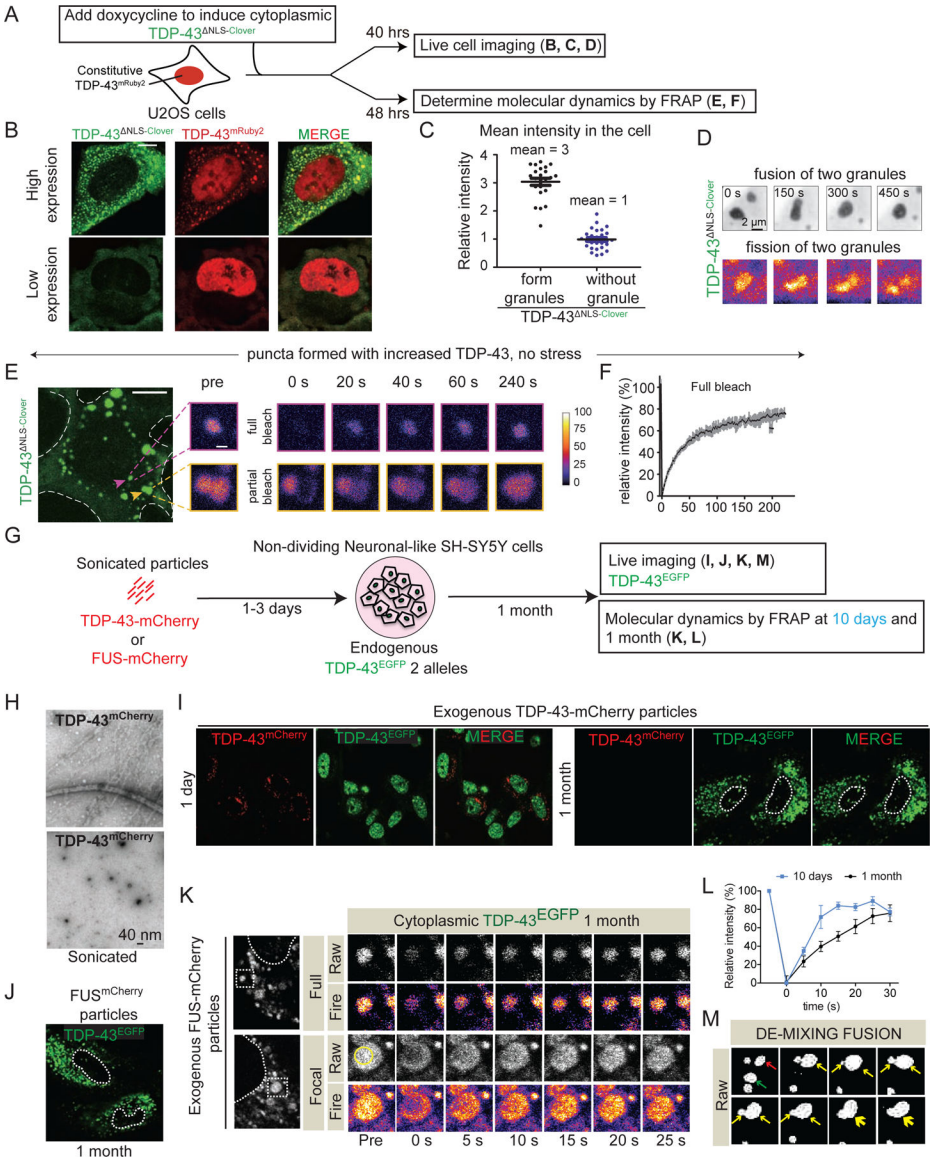

Figure 2. Fluorescently tagged TDP-43 de-mixes in the cytoplasm forming liquid-like droplets that are dynamic and fuse.

(A) Schematic of experimental design to assess LLPS properties of cytoplasmic TDP-43 with increasing TDP-43 levels. (B) U2OS cells expressing high and low levels of cytoplasmic TDP-43$^{\Delta NLS\text{-}Clover}$ and nuclear TDP-43^{mRuby2}. (C) Relative fluorescence intensity of cytoplasmic TDP-43$^{\Delta NLS\text{-}Clover}$ in cells with (black dots) or without (blue dots) cytoplasmic TDP-43 particles. (D) Representative fusion and fission event of cytoplasmic TDP-43 liquid-like droplets. (E) Representative cytoplasmic TDP-43$^{\Delta NLS\text{-}Clover}$ particles (green) formed with increased accumulated levels of TDP-43 in absence of stress (left). FRAP examples of fully (upper panel) or partially (lower panel) bleached TDP-43$^{\Delta NLS\text{-}Clover}$ particles. (F) Mean fluorescence intensity of the fully bleached TDP-43$^{\Delta NLS\text{-}Clover}$ particle over time, normalized to the average intensity of the particle before photobleaching (and represented as mean ± SEM from the recovery curves of six droplets in a total of three independent experiments). See also Figure S3. (G) Experimental

design to assess LLPS properties of endogenously EGFP tagged TDP-43 expressed from both endogenous TDP-43 alleles in non-cycling SH-SY5Y cells after incubation with wild-type TDP-43^{mCherry} or FUS^{mCherry} fibrils and visualized over time by live-imaging. (H) Electron micrographs of amyloid-like fibrils of full-length wild-type TDP-43^{mCherry}. Bottom panel illustrates the TDP-43^{mCherry} fibrils after sonication before inoculating them into cell media. (I) Representative images of neuronal-like SH-SY5Y cells inoculated with sonicated TDP-43^{mCherry} fibrils at a final concentration of 200nM and further imaged for TDP-43^{mCherry} particles (red) and TDP-43^{EGFP} (green) up to 1 month. Media were changed after 3 days. Dashed white line outlines nuclei. (J) Neuronal-like SH-SY5Y cells imaged for direct GFP fluorescence from TDP-43^{EGFP} (green) 1 month after transient incubation with sonicated FUS^{mCherry} particles. (K) Cytoplasmic droplets of TDP-43^{EGFP} expressed from both endogenous TDP-43 alleles (left panel). FRAP examples of fully or partially bleached TDP-43^{EGFP} droplets. (L) Mean fluorescence intensity of the fully bleached TDP-43^{EGFP} droplets over time at 10 days or 1 month, normalized to average particle intensity before photobleaching (represented as mean ± SEM from the recovery curves of 8 droplets in a total of three independent experiments). (M) Fusion event between two cytoplasmic TDP-43^{EGFP} droplets. Arrows point to two particles (red and green) that initially fused into one (yellow arrow) at minute 2. At minute 4 another particle (new yellow arrow) fused to the newly formed LLPS at minute 12 (large yellow arrow). See also Figure S2.

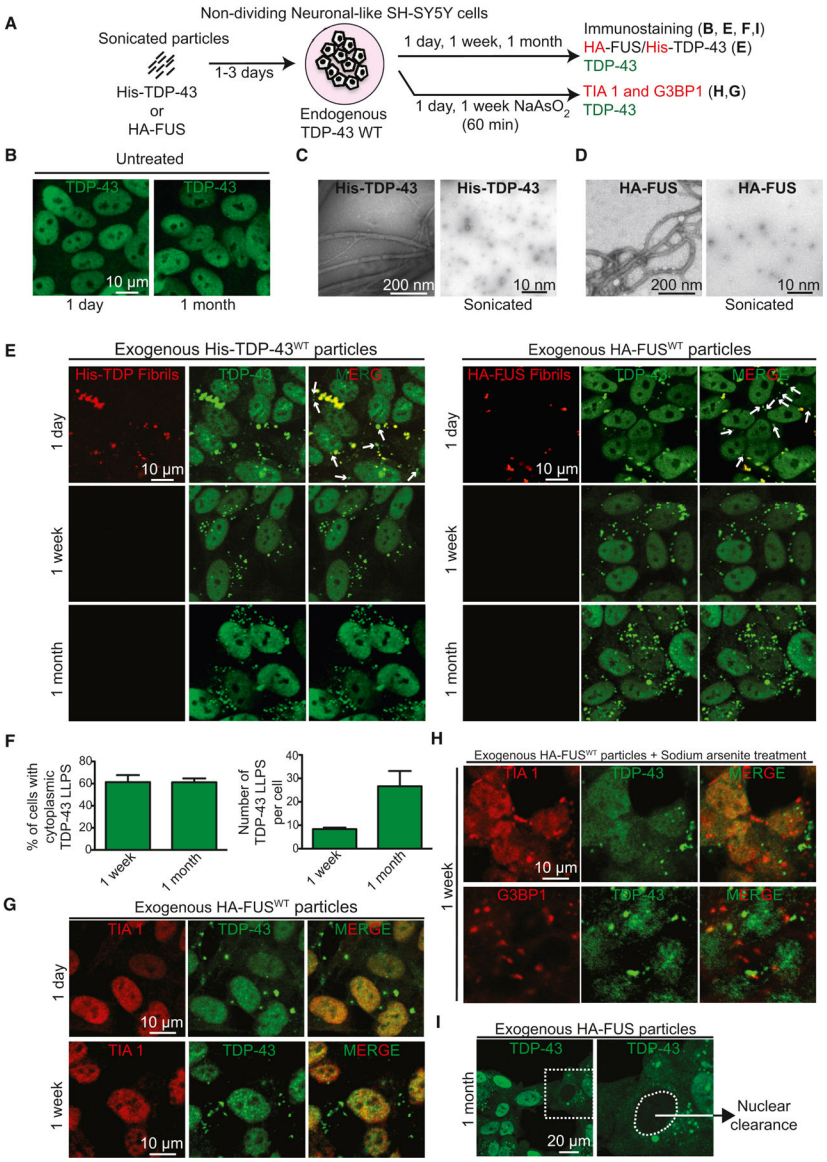

Figure 3. Transient stress induces long-lasting untagged, cytosolic TDP-43 particles independent of conventional stress granules.

(A) Schematic of experimental design to assess endogenous wild type TDP-43 de-mixing in the cytoplasm of neuronal-like SH-SY5Y cells (non-cycling). (B) Representative images of endogenous nuclear TDP-43 in non-fibril-treated SH-SY5Y cells at day 1 (left) and after one month of culture (right). (C-D) Electron micrographs of amyloid-like fibrils of full-length wild-type His-TDP-43 (C) or HA-FUS (D) purified from bacteria. Respective right panels illustrate the His-TDP-43 or HA-FUS fibrils after sonication before inoculating them into cell media. (E) Representative images of neuronal-like SH-SY5Y cells after 1 day, 1 week or 1 month after inoculated sonicated His-TDP-43 (left) or HA-FUS fibrils (right) at a final concentration of 200nM and immunostained with His- or HA-tag (red) and TDP-43 (green) antibodies. Media was changed after 3 days. White arrows indicate cytoplasmic particles containing endogenous wild-type TDP-43 (green). (F) Quantification of the number of cells with cytoplasmic de-mixed TDP-43 over time (left panel). (Right panel) Quantification of

cytoplasmic particles per cell with time (represented as mean ± SEM from 200 cells in a total of three independent experiments). (G-H) Representative images of SH-SY5Y cells incubated with sonicated HA-FUS particles and (G) immunostained after 1 day (top panel) or 1 week (bottom panel) with stress granule marker TIA1 (red) and TDP-43 (green) antibodies or (H) after treatment with $NaAsO_2$ (0.5 mM) for 1 hour and immunostained with TIA1 or G3BP1 (red) and TDP-43 (green) antibodies. (I) Representative images of SH-SY5Y cells with apparent cytoplasmic TDP-43 de-mixing accompanied by depletion of nuclear TDP-43 1-month post-treatment with sonicated HA-FUS particles. Higher magnification of the white boxed area in the left panel (right panel). The white dashed line outlines the nucleus. See also Figure S3.

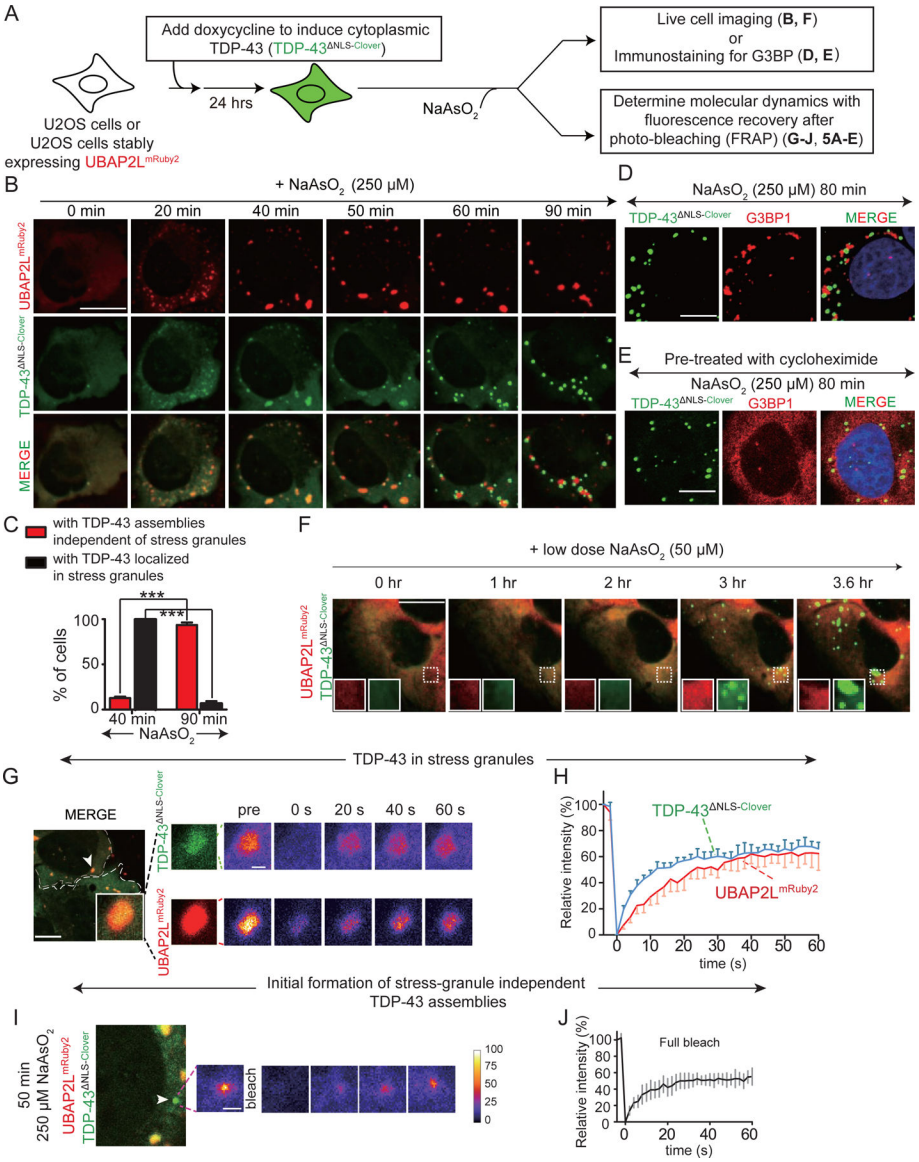

Figure 4. Arsenite induces cytoplasmic TDP-43 de-mixing into round, liquid-likecompartments that are distinct from stress granules.

(A) Schematic of experimental design to assess the relationship of cytoplasmic TDP-43 with stress granules (TDP-43$^{\Delta NLS\text{-}Clover}$) in the presence of sodium arsenite. (B) Representative images of U2OS cells co-expressing stress granule protein UBAP2L^{mRuby2} and cytoplasmic TDP-43 (TDP-43$^{\Delta NLS\text{-}Clover}$) after addition of 250 μM $NaAsO_2$. White arrowheads indicate round TDP-43 particles independent of stress granules after 50 minutes of $NaAsO_2$ treatment. (C) Quantification of TDP-43 recruitment to stress granules and cells that show formation of stress granule independent TDP-43 assemblies (from five independent frames in a live imaging experiment, total cell number from each frame = 25, 12, 30, 16, 10, respectively). Data are shown as box whisker plot (showing mean, min and max values). ***: P<0.001, paired t test. (D) Endogenous stress granules [using G3BP1 antibody (red)] in cells expressing cytoplasmic TDP-(TDP-43$^{\Delta NLS\text{-}Clover}$; green) after treatment with $NaAsO_2$ for 80 minutes. (E) Endogenous G3BP1 (red) in cells expressing TDP-43$^{\Delta NLS\text{-}Clover}$ (green)

after pre-treatment with cycloheximide (10 μg/mL) followed by $NaAsO_2$ treatment for 80 minutes. (F) Representative images of U2OS cells co-expressing stress granule protein $UBAP2L^{mRuby2}$ and cytoplasmic TDP-43 ($TDP\text{-}43^{\Delta NLS\text{-}Clover}$) after addition of 50 μM $NaAsO_2$. (G) FRAP of $TDP\text{-}43^{\Delta NLS\text{-}Clover}$ (green) and $UBAP2L^{mRuby2}$ (red) in a stress granule. (H) Mean fluorescence intensity of $TDP\text{-}43^{\Delta NLS\text{-}Clover}$ and $UBAP2L^{mRuby2}$ plotted over time (normalized to average intensity of a droplet before photobleaching and represented as mean ± SEM from the recovery curves of a total of four granules from two independent FRAP experiments). (I) FRAP example of an initial stage formation of a cytoplasmic $TDP\text{-}43^{\Delta NLS\text{-}Clover}$ (green) droplet independent of the stress granules $UBAP2L^{mRuby2}$ (red). (J) Mean fluorescence intensity of $TDP\text{-}43^{\Delta NLS\text{-}Clover}$ droplet (indicated by white arrowhead) plotted over time (lower graph). Data are normalized to the average intensity of a droplet before photobleaching (and are represented as mean ± SEM from the recovery curves of four droplets in a total of three independent experiments). See also Figure S4.

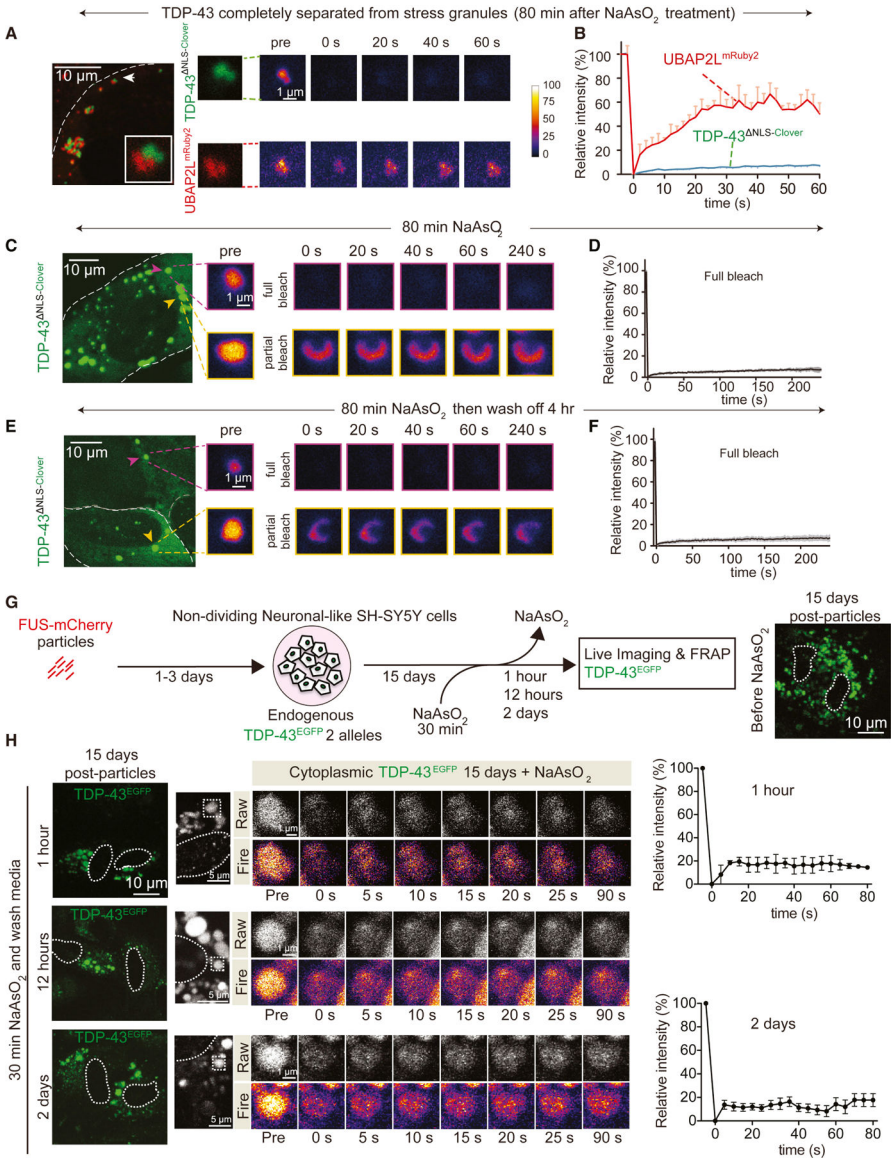

Figure 5. Arsenite induces liquid-liquid phase separation of cytoplasmic TDP-43 that quickly converts into a gel/solid state.

(A) Representative image using confocal microscopy of TDP-43$^{\Delta NLS\text{-}Clover}$ particles that are independent of UBAP2L^{mRuby2} stress granules after 80 minutes of $NaAsO_2$ treatment (left). FRAP example of the TDP-43$^{\Delta NLS\text{-}Clover}$ particle (green) and UBAP2L granule (red) shown in the white box (of the left image). (B) Mean fluorescence intensity of a TDP-43$^{\Delta NLS\text{-}Clover}$ particle and a UBAP2L^{mRuby2} granule plotted over time. Data are normalized to the average intensity of a particle before photobleaching and are represented as mean ± SEM from the recovery the curves of five particles in a total of two independent experiments. (C) Representative of cytoplasmic TDP-43$^{\Delta NLS\text{-}Clover}$ particles (green) after 80 minutes of $NaAsO_2$ treatment (left). FRAP examples of fully (upper panel) or partially (lower panel) bleached TDP-43$^{\Delta NLS\text{-}Clover}$ particles. (D) Mean fluorescence intensity of the fully bleached TDP-43$^{\Delta NLS\text{-}Clover}$ particle over time. Data are normalized to the average intensity of a particle before photobleaching and are represented as mean ± SEM from the recovery curves

of five particles in a total of two independent experiments. (E) Representative image of cytoplasmic TDP-43$^{\Delta NLS\text{-}Clover}$ particles (green) after minutes of $NaAsO_2$ treatment followed by a 4-hour wash of arsenite (left). FRAP examples of fully (upper panel) or partially (lower panel) bleached TDP-43$^{\Delta NLS\text{-}Clover}$ particles. (F) Mean fluorescence intensity of the fully bleached TDP-43$^{\Delta NLS\text{-}Clover}$ particle over time. Data are normalized to the average intensity of a particle before photobleaching and are represented as mean ± SEM from the recovery curves of seven particles in a total of two independent experiments. (G) Schematic of experimental design to assess LLPS properties of endogenous TDP-43^{EGFP} in cells treated for 2 weeks with FUS particles and sodium arsenite. (H) Representative images of cytoplasmic endogenous TDP-43^{EGFP} particles after 30 minutes of sodium arsenite addition in cells treated with FUS particles for 2 weeks (left panel). FRAP examples of TDP-43^{EGFP} particles fully bleached. Mean fluorescence intensity of the fully bleached TDP-43^{EGFP} particles over time (right). Data are normalized to the average intensity of a particle before photobleaching and is represented as mean ± SEM from the recovery curves of 4 particles in a total of three independent experiments. See also Figure S5.

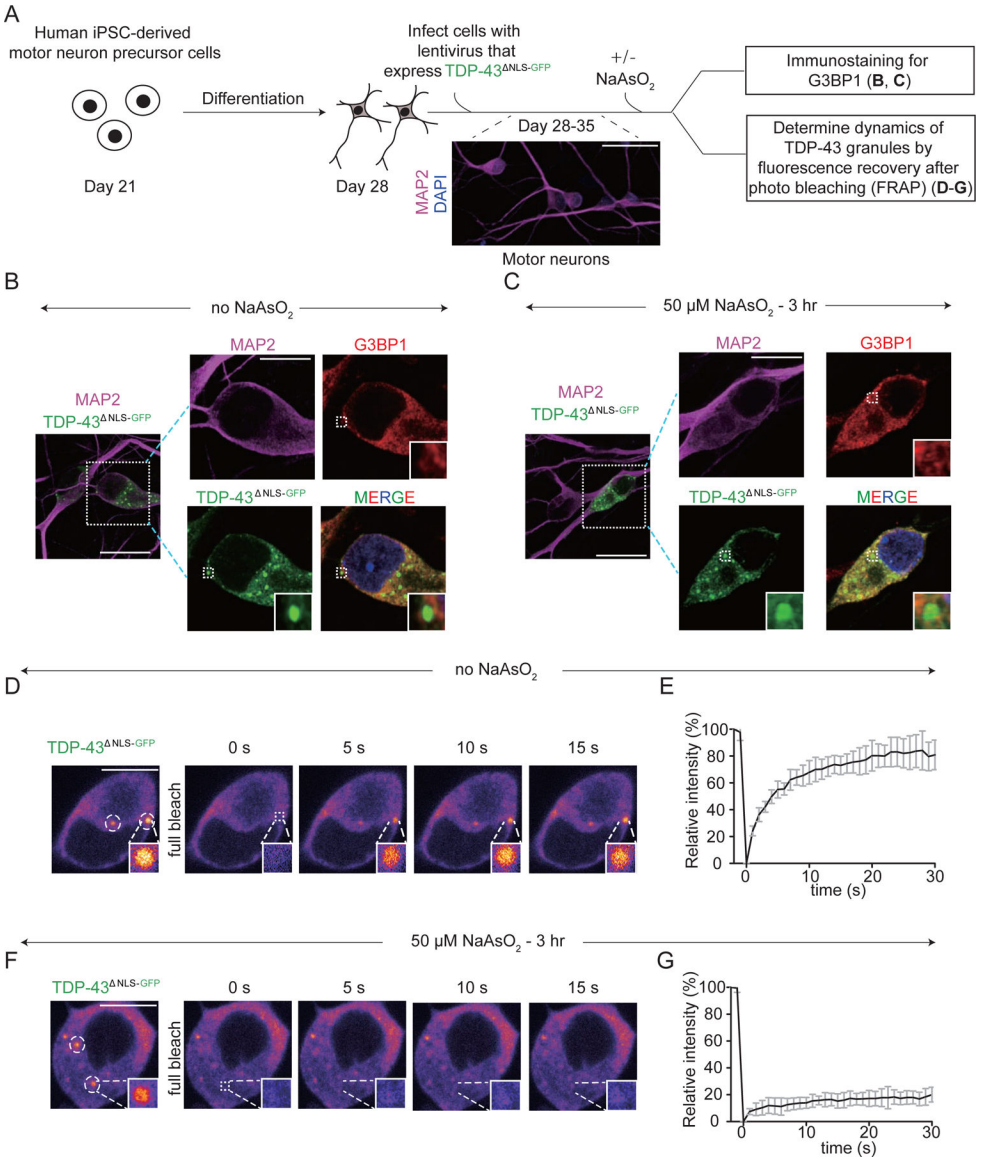

Figure 6. De-mixing of cytoplasmic TDP-43 in human iPSC-derived motor neurons forms liquid-like droplets independent of stress granules, which convert into a gel/solid-like state after arsenite induced stress.

(A) Schematic of experimental design to assess the properties of de-mixed cytoplasmic TDP-43 particles in human iPSC-derived motor neurons with or without sodium arsenite treatment. Human iPSC-derived motor neuron precursor cells were differentiated for 7 days and then the differentiated motor neurons were infected with a lentivirus driving expression of Ubi::TDP-43$^{\Delta NLS\text{-}GFP}$. After 1–2 weeks of expression the cells were analyzed. (B-C) Immunostaining of G3BP1 of mature motor neurons expressing cytoplasmic TDP-43 in absence of sodium arsenite treatment (B) or with 50 μM sodium arsenite (C). MAP2 was stained for neuron marker. (D-E) Representative images of cytoplasmic TDP-43$^{\Delta NLS\text{-}GFP}$ particles formed in absence of stress. FRAP example of TDP-43$^{\Delta NLS\text{-}GFP}$ particles in a neuron after a complete bleaching. (E) Mean fluorescence intensity of the fully bleached TDP-43$^{\Delta NLS\text{-}GFP}$ particles over time. Data are normalized to the average intensity of a

particle before photobleaching and are represented as mean ± SEM from the recovery curves of 8 particles in a total of four independent experiments. (F-G) Representative images of cytoplasmic TDP-43$^{\Delta NLS\text{-}GFP}$ particles after 3 hours of 50 μM sodium arsenite treatment. FRAP example of TDP-43$^{\Delta NLS\text{-}GFP}$ particles in a motor neuron after a complete bleaching. (G) Mean fluorescence intensity of the fully bleached TDP-43$^{\Delta NLS\text{-}GFP}$ particles over time. Data are normalized to the average intensity of a particle before photobleaching and are represented as mean ± SEM from the recovery curves of nine particles in a total of four independent experiments.

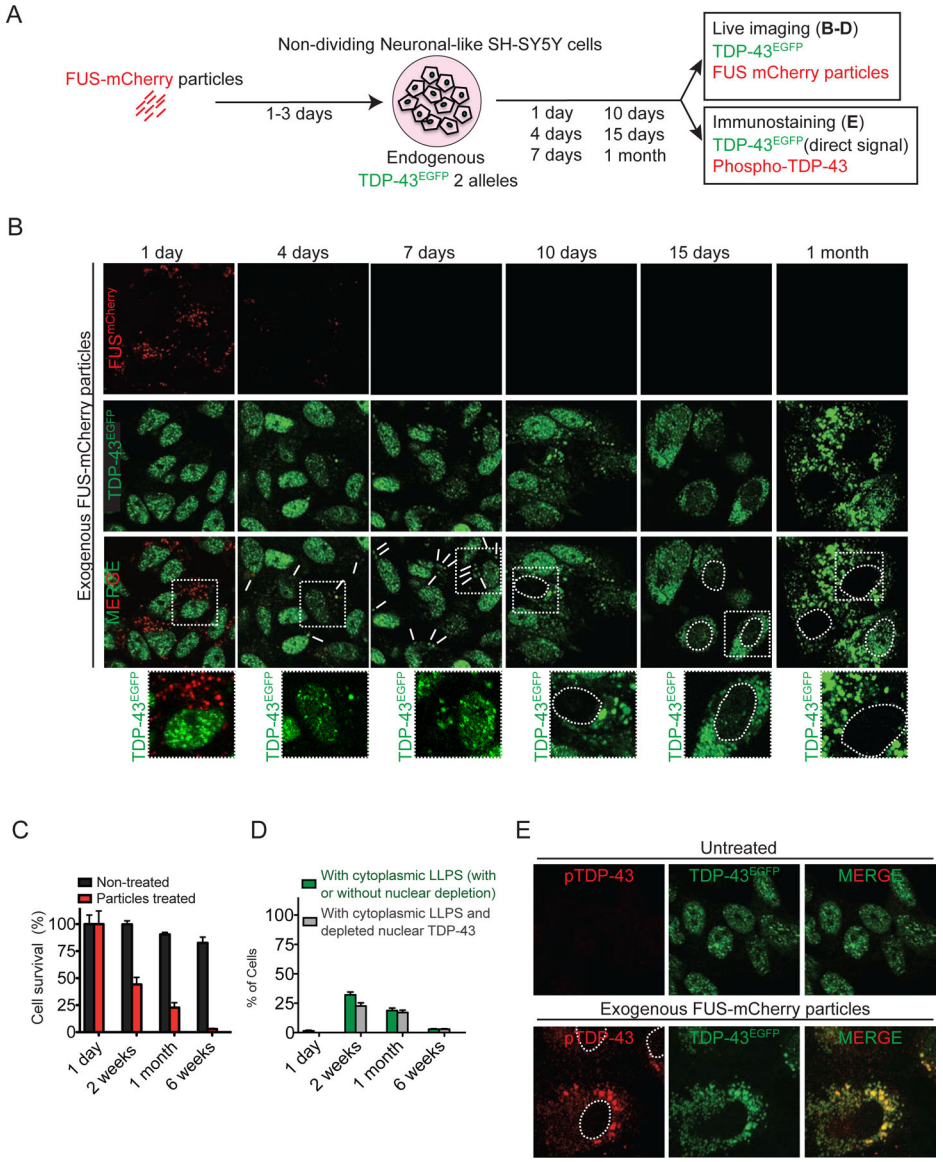

Figure 7. Endogenous EGFP-tagged TDP-43 de-mixes in the cytoplasm, forming liquid-like droplets which slowly deplete nuclear TDP-43 and compromise cell survival.

(A) Schematic of experimental design to assess LLPS properties of endogenously EGFP tagged TDP-43 in non-cycling SH-SY5Y cells (knock-in in both alleles), which were incubated with fluorescently labelled wild type $FUS^{mCherry}$ fibrils and visualized over time by live-imaging or immunofluorescence. (B) Representative images using confocal microscopy of neuronal-like SH-SY5Y cells inoculated with sonicated His-$FUS^{mCherry}$ particles at a final concentration of 200nM and further imaged for $FUS^{mCherry}$ fibrils (red) and TDP-43^{EGFP} (green) up to 1 month. Media was changed after 3 days. White arrows indicate cytoplasmic particles containing mislocalized endogenous TDP-43^{EGFP} (green). Dashed white line outlines nuclei. (C) Cell survival quantification of non-treated (black) and fibril-treated (red) neuronal-like cells over time. Data are represented as mean ± SEM from a total of three independent experiments. (D) Quantification of the percentage of cells with cytoplasmic LLPS (with or without nuclear TDP-43 clearance) (green), or with cytoplasmic

LLPS accompanied by nuclear clearance (gray). Data are represented as mean ± SEM from a total of three independent experiments. (E) Representative images of neuronal-like SH-SY5Y cells 1 month after inoculation of sonicated $FUS^{mCherry}$ fibrils and further immunostained with phospho-TDP-43 (red) and cytoplasmic $TDP\text{-}43^{EGFP}$ (green). See also Figure S6.

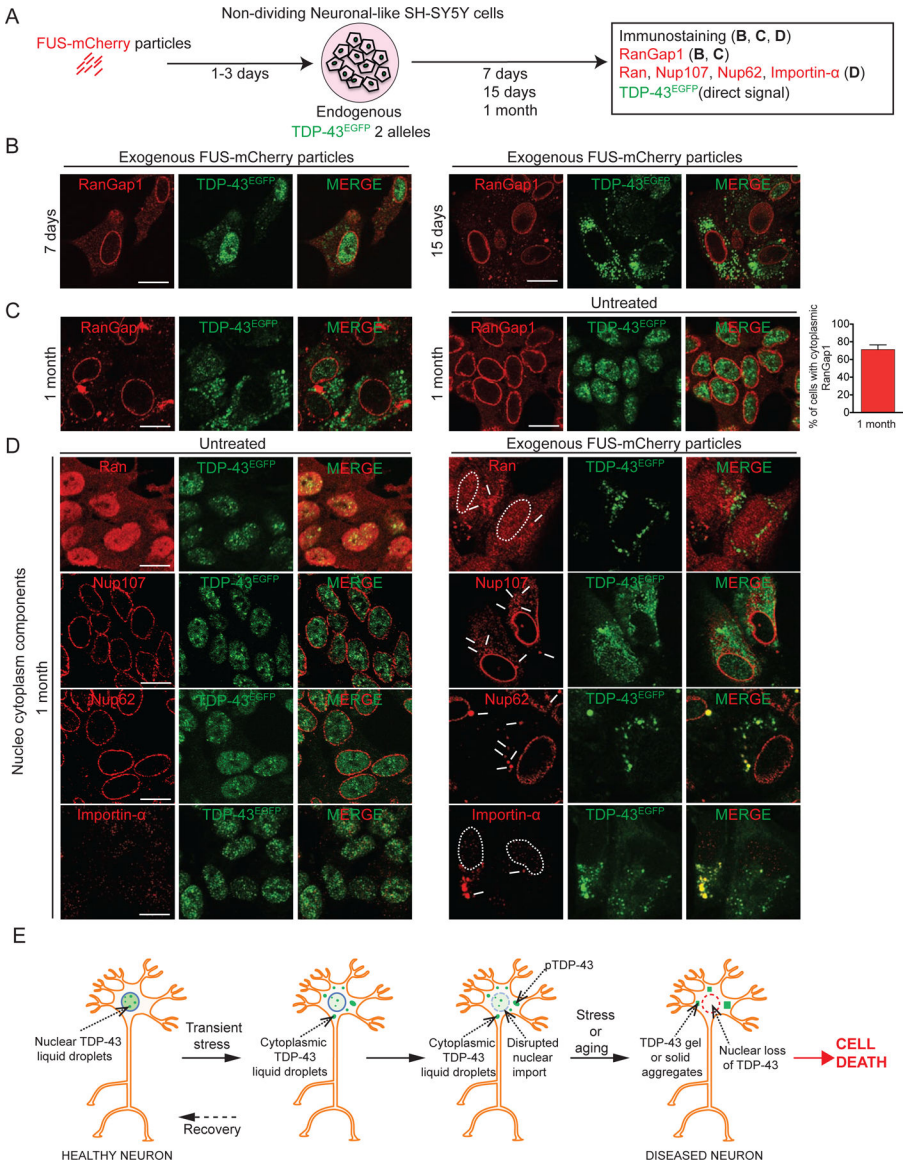

Figure 8. TDP-43 LLPS is accompanied by disruption of nucleocytoplasmic transport.

(A) Schematic of experimental design to assess LLPS properties of endogenous TDP-43^{EGFP} in cells and their impact on nucleocytoplasmic transport. (B) Representative images using confocal microscopy of neuronal-like SH-SY5Y cells 7 days and 15 days post-incubation of sonicated FUS^{mCherry} fibrils and further immunostained with RanGap1 (red) and cytoplasmic TDP-43^{EGFP} (green). (C) Immunostained RanGap1 (red) and cytoplasmic TDP-43^{EGFP} (green) 1 month after incubation with FUS^{mCherry} sonicated fibrils or in absence of fibril-treatment (right panel). Quantification of the percentage of cells with cytoplasmic RanGap1 inclusions 1 month post-treatment (from 200 cells in a total of three independent experiments). (D) Representative images 1 month post-incubation and further immunostained with Ran (upper panel), Nup107 (second panel), Nup62 (third panel) and Importin-α (lower panel) (red) together with cytoplasmic TDP-43^{EGFP} (green). See also Figure S7. (E) Schematic of how transient stress can induce cytoplasmic TDP-43 LLPS,

disruption in nuclear import, accumulation of phospho-TDP-43, conversion from a de-mixed liquid to a gel/solid, depletion with time of nuclear TDP-43, and ultimately cell death.

KEY RESOURCE TABLE

REAGENT or RESOURCE	SOURCE	IDENTIFIER
Antibodies		
Rabbit anti-TDP-43 (polyclonal)	Proteintech	Cat# 10782–2-AP, RRID: AB_615042
Rabbit anti-TDP-43 (polyclonal)	Proteintech	Cat# 12892–1-AP, RRID: AB_2200505
Mouse anti-GFP (monoclonal, JL-8)	Clontech	Cat# 632381, RRID: AB_2313808
Mouse anti-G3BP1 (monoclonal)	Abcam	Cat# ab56574, RRID: AB_941699
Goat anti-TIA1 (polyclonal)	Santa Cruz	Cat# sc-1751, RRID: AB_2201433
Mouse anti-HA (monoclonal, HA.11)	Covance	Cat# mms-101P, RRID: AB_2314672
Rat anti-tubulin (monoclonal)	Abcam	Cat# ab6160, RRID: AB_305328
Mouse anti-GAPDH (monoclonal)	Abcam	Cat# ab8245, RRID: AB_2107448
Rat anti-phospho-TDP-43	Biolegend	Cat# 829901, RRID: AB_2564934
Goat anti-RanGap1	Santa Cruz	Cat# sc-1862, RRID: AB_2176981
Mouse anti-Ran	BD Bioscience	Cat# bd-610340, RRID: AB_397730
Rabbit anti-Nup107	Abcam	Cat# Ab73290, RRID: AB_1269604
Goat anti-FUS	Bethyl Laboratories	Cat# A303–839A, RRID: AB_2620190
Mouse anti-hnRNPA1	Santa Cruz	Cat# sc-374053, RRID: AB_10947257
Rabbit anti-amyloid A11	ThermoFisher	Cat# AHB0052, RRID: AB_1501357
Rabbit anti-peIF2a	Cell Signaling	Cat# 3398, RRID: AB_2096481
Guinea pig anti-p62	Progen	Cat# GP62-C, RRID: AB_2687531
Mouse anti-EDC4	Santa Cruz	Cat# sc-376382, RRID: AB_10988077
Mouse anti-ubiquitin	Millipore	Cat# MAB1510, RRID: AB_2180556
Mouse anti-Importin alpha 2	Novus Biologicals	Cat# MAB6207, RRID: AB_10730707
Chicken MAP2	Novus Biologicals	Cat# NB300–213 RRID:AB_2138178
Bacterial and Virus Strains		
E. coli DH 5-alpha competent cells	New England Biolabs	Cat# 2981I
E. coli BL21 competent cells	EMD millipore	Cat# **69450–3**
Biological Samples		
Chemicals, Peptides, and Recombinant Proteins		
Protamine sulfate	Sigma-Aldrich	Cat# P4020
TransIT-X2 transfection reagent	Mirus	Cat# MIR 6000

REAGENT or RESOURCE	SOURCE	IDENTIFIER
Sodium arsenite	Sigma-Aldrich	Cat# 1062771000
PD 0332991 (Palbociclib)	Apexbio	Cat# PD-0332991
Carbonic Anhydrase from bovine erythrocytes	Sigma-Aldrich	Cat# C2273–1VL
Albumin, bovine serum	Sigma-Aldrich	Cat# A8531
B-Amylase from sweet potato	Sigma-Aldrich	Cat# A8781
TEV protease	ThermoFisher	Cat# 12575015
Poly-D-lysine	Sigma-Aldrich	Cat# P0899
Laminin	Corning	Cat# 354232
20% paraformaldehyde solution, EM grade	Fisher Scientific	Cat# 15713S
Neomycin	Thermo Fisher	Cat# 10131035
Blasticidin	Thermo Fisher	Cat# A1113903
Puromycin Dihydrochloride	Thermo Fisher	Cat# A1113803
Doxycycline	Sigma-Aldrich	Cat# D9891–5G
Uranyl acetate	Ladd R.I., Williston, VT	Cat# 23620
Antibiotic-Antimycotic	Thermo Fisher	Cat# 15240062
Fetal Bovine Serum	Omega Scientific	Cat# FB-01
Critical Commercial Assays		
Deposited Data		
Experimental Models: Cell Lines		
iPS Cells	iXCells	N/A
Human: SH-SY5Y	ATCC	Cat# CRL-2266
Human: SH-SY5Y TDP-43$^{AID-GFP}$	This paper	N/A
Human: U2OS	ATCC	Cat# HTB-96
Human: HEK293T	ATCC	Cat# CRL-3216
Experimental Models: Organisms/Strains		
C57BL/6 (C57BL/6 NCrL) mice	Charles River Laboratories	Cat# C57BL/6NCrl
Oligonucleotides		

REAGENT or RESOURCE	SOURCE	IDENTIFIER
Synthetic RNA poluCUG repeat (5X)	IDT	N/A
Oligo-dT(20)	Gift from Dr. J. Paul Taylor (St. Jude Children Hospital)	N/A
Recombinant DNA		
pDUET-HA-FUS^{WT}	This paper	N/A
pET His-TDP-43^{WT}	This paper	N/A
pET His-SOD1^{A4V}	This paper	N/A
pRK2- His-FUS^{WT}-mCherry	This paper	N/A
pRK2-His-TDP-43^{WT}-mCherry	This paper	N/A
pRK2-His-TDP-43^{G298S}-mCherry	This paper	N/A
pRK2-His-SOD1^{G93R}-mCherry	This paper	N/A
pX330-U6-Chimeric_BB-CBh-hSpCas9	Addgene Cat# 42230	(Cong et al., 2013)
Lentivirus		
EF1a-Tet3G-IRES-Neo	This paper	N/A
Ubic-myc-TDP-43^{WT}-mRuby2-SV40-Puro	This paper	N/A
TRE3G-TDP-43$^{\Delta NLS(K82A,R83A,K84A)1-414}$-Clover-EF1acore-BSD	This paper	N/A
Ubic-UBAP2L-mRuby2-SV40-Puro	This paper	N/A
Ubic-TDP-43$^{\Delta NLS(K82A,R83A,K84A)1-414}$-Clover-SV40-Puro	This paper	N/A
pCDH-CMVtet-EYFP-TDP-43	This paper	N/A
Software and Algorithms		
FIJI (ImageJ)	NIH	Fiji, RRID: SCR_002285 https://fiji.sc/#download
Benchlin webtool	Benchling	https://benchling.com/signup
Graphpad prism	Graphpad	Graphpad Prism RRID:SCR_002798 https://www.graphpad.com/scientific-software/prism/
Other		
96 well glass bottom plate	Cellvis	Cat# P96–1.5H-N
8 well chamber slides (glass bottom)	Ibidi	Cat# 80827
GSTrap HP columns	GE	Cat# 17–5281-01
HisTrapHP colums	GE	Cat# 7–5248-02
Superdex 75 10/300	GE	Cat# 17–5174-01
Sephadex G-25 in PD-10	GE	Cat# 17–0851-01
Hemacytometer	Fisher Scientific	Cat# 267110
DeltaVision Core system	GE	N/A

REAGENT or RESOURCE	SOURCE	IDENTIFIER
Olympus FV1000 Spectral Confocal with SIM Scanner	Olympus	N/A
Tecnai G2 Spirit BioTWIN transmission electron microscope equipped	Tecai	N/A
Zeiss LSM 880 confocal microscope	Zeiss	N/A
CQ1 confocal quantitative image cytometer	Yokogawa	N/A
SH800S Sony cell sorter	Sony	N/A
JEOL 1200 EX II TEM	JEOL USA	N/A
Akta Pure	GE	N/A
Amaxa Nucleofactor	Lonza	N/A
C-B 300 mesh Cu-01813-F	Ted pella	Cat# Cu-01813-F